

# Spectral Properties of the Anderson Impurity Model: Comparison of Numerical Renormalization Group and Non-Crossing Approximation

T. A. Costi<sup>1</sup>, J. Kroha<sup>2</sup> and P. Wölfle<sup>1</sup>

<sup>1</sup> *Universität Karlsruhe, Institut für Theorie der Kondensierten Materie, 76128 Karlsruhe,  
Germany*

<sup>2</sup> *Cornell University, LASSP, Ithaca, N.Y. 14853, U.S.A.*

## Abstract

A comparative study of the numerical renormalization group and non-crossing approximation results for the spectral functions of the  $U = \infty$  Anderson impurity model is carried out. The non-crossing approximation is the simplest conserving approximation and has led to useful insights into strongly correlated models of magnetic impurities. At low energies and temperatures the method is known to be inaccurate for dynamical properties due to the appearance of singularities in the physical Green's functions. The problems in developing alternative reliable theories for dynamical properties have made it difficult to quantify these inaccuracies. In this paper we show, by direct comparison with essentially exact numerical renormalization group calculations for the auxiliary and physical particle spectral functions, that the main source of error in the non-crossing approximation is in the lack of vertex corrections in the convolution formulae for physical Green's functions. We show that the dynamics of the auxiliary particles within NCA is essentially correct for a large parameter region, including the physically interesting Kondo regime, for all energy scales down to  $T_0$ , the low energy scale of the model and often well below this scale. Despite the satisfactory description of the

auxiliary particle dynamics, the physical spectral functions are not obtained accurately on scales  $\sim T_0$ . Our results suggest that self-consistent conserving approximations which include vertex terms may provide a highly accurate way of dealing with strongly correlated systems at low temperatures.

PACS numbers: 71.27.+a,71.28.+d,72.20.Hr

## I. INTRODUCTION

In recent years the physics of strongly correlated Fermi systems has attracted wide interest, in particular in the context of high  $T_c$  superconductors [1] and their normal state properties [2]. Despite intense efforts, systematic and controlled theoretical methods for dealing with such systems are still lacking. At the heart of the problem is the effect of a strong on-site Coulomb repulsion  $U$  on fermions living on a lattice, in particular in  $d = 2$  dimensions. At low energy such models can be mapped onto effective Hamiltonians with the constraint of no double occupancy of any lattice sites. The projection onto the corresponding subspace of Hilbert space is presumably responsible for a number of unusual properties, most remarkably the spin-charge separation and non-Fermi liquid behaviour. Unfortunately the local constraints on the site occupancy are difficult to handle. One possible formulation [3] uses auxiliary particles such as slave-bosons ( $b$ ) and pseudo-fermions ( $f_\sigma$ ) to represent an electron as a composite particle consisting of a pseudo-fermion particle and a slave-boson hole ( $f_\sigma^\dagger b$ ). The local constraint is holonomic in this formulation, and is given by the condition that the sum of the occupation numbers of pseudo-fermions and slave-bosons is equal to unity at any lattice site,  $\sum_\sigma n_{f_\sigma} + n_b = 1$ . The constraint is closely related to the local gauge symmetry of the system with respect to simultaneous  $U(1)$  gauge transformations of  $b$  and  $f_\sigma$ . It may be shown that starting with certain mean field theories the constraint and its consequences lead to the appearance of longitudinal and transverse fictitious gauge fields coupling equally to pseudo-fermions and slave-bosons [4]. The gauge fields restore the local symmetry broken in mean field theory.

However, it is not clear that the slave-boson mean field theories are a good starting point (except for the cases where a physical phase transition into a magnetic or superconducting phase takes place). Alternatively one may guarantee the local gauge invariance of approximations by deriving those from a generating functional [5]. The local gauge invariance ensures conservation of the local occupation at each lattice site (the “local charge”) in time. In order to effect the actual projection, it is still necessary to fix the occupation numbers

at a given time locally. So far this has only been achieved for impurity models, e.g. the Anderson model of a magnetic impurity in a metallic host [6–8].

Even if the projection is done exactly, an equally important question is the selection of the dominating contributions in perturbation theory in the hybridization (or in the hopping integrals and exchange interaction in the case of lattice models). In this paper we address this question for the infinite U Anderson impurity model (degeneracy  $N = 2$ ). We employ the numerical renormalization group (NRG) to calculate the slave-boson and pseudo-fermion spectral functions and compare the results with those of the simplest fully projected conserving approximation, the so called “non-crossing approximation” (NCA) [9,10]. While the NCA is known to give excellent results for large degeneracy  $N$  and not too low temperatures, including the cross-over from low ( $T \ll T_K$ ) to high temperature ( $T \gg T_K$ , where  $T_K$  is the Kondo temperature) [7,10], pronounced deviations from exactly known results appear at  $N = 2$  [8,11]. The comparisons will allow us to pinpoint the deficiencies of the NCA and to identify possible improvements.

In earlier publications [12,13] we have presented results of an NRG calculation of the slave-boson and pseudo-fermion spectral functions at zero temperature. We found these functions to be infrared divergent at threshold, with critical exponents dependent on the d-level occupancy  $n_d$  and given by simple expressions identical to the well known X-ray absorption threshold exponents.

The paper is organized as follows: In Section II we formulate the model, describe how we implement the numerical renormalization group for studying auxiliary spectral functions of this model and describe the NCA within the framework of conserving approximations. Section III describes our results for spectral functions calculated with the above two methods. In Section IV we summarize our main results. Some details of the auxiliary particle technique, which make it suitable for an effective evaluation at the lowest temperatures, are discussed in the appendices.

## II. FORMULATION

### A. Model and Application of the Renormalization Group

The Anderson model of an impurity  $d$  electron state hybridizing with the conduction band with infinitely strong Coulomb repulsion in the  $d$ -level in auxiliary particle representation takes the form

$$H = H_c + \epsilon_d \sum_{\sigma} f_{\sigma}^{\dagger} f_{\sigma} + V \sum_{\sigma} (c_{0\sigma}^{\dagger} b^{\dagger} f_{\sigma} + h.c.), \quad (1)$$

where  $H_c = \sum_{k\sigma} \epsilon_k c_{k\sigma}^{\dagger} c_{k\sigma}$  is the conduction electron kinetic energy and  $c_{0\sigma} = \sum_k c_{k\sigma}$  annihilates a conduction electron with spin  $\sigma$  at the impurity site 0. The Hilbert space consists of disjoint subspaces characterized by the conserved auxiliary particle number  $Q = b^{\dagger} b + \sum_{\sigma} f_{\sigma}^{\dagger} f_{\sigma}$ ,  $Q = 0, 1, 2, \dots$ . The physical subspace is defined by the constraint  $Q = 1$ . Following Wilson [14] we (i) linearize the spectrum of  $H_c$  about the Fermi energy  $\epsilon_k \rightarrow k$ , (ii) introduce a logarithmic mesh of  $k$  points  $k_n = \Lambda^{-n}$  and (iii) perform a unitary transformation of the  $c_{k\sigma}$  such that  $c_{0\sigma}$  is the first operator in the new basis and  $H_c$  takes the form of a tight-binding Hamiltonian in  $k$ -space,

$$H_c = \sum_{n=0}^{\infty} \sum_{\sigma} \xi_n \Lambda^{-n/2} (c_{n+1\sigma}^{\dagger} c_{n\sigma} + h.c.), \quad (2)$$

with  $\xi_n \rightarrow (1 + \Lambda^{-1})/2$  for  $n \gg 1$ . These steps are explained in detail in [14] and can be taken over for the present model without change.

The Hamiltonian (1) together with the discretized form of the kinetic energy (2) in the new basis is now diagonalized by the following iterative process: (i) one defines a sequence of finite size Hamiltonians  $H_N$  by replacing  $H_c$  in (2) by  $H_N^c = \sum_{n=0}^{N-1} \sum_{\sigma} \xi_n \Lambda^{-n/2} (c_{n+1\sigma}^{\dagger} c_{n\sigma} + h.c.)$ ; (ii) starting from  $H_0 = \epsilon_d \sum_{\sigma} f_{\sigma}^{\dagger} f_{\sigma} + V \sum_{\sigma} (c_{0\sigma}^{\dagger} b^{\dagger} f_{\sigma} + h.c.)$ , each successive hopping may be considered as a perturbation on the previous Hamiltonian; (iii) the Hamiltonians  $H_N$  are scaled such that the energy spacing remains the same. This defines a renormalization group transformation  $\bar{H}_{N+1} = \Lambda^{1/2} \bar{H}_N + \xi_N \sum_{\sigma} (c_{N+1\sigma}^{\dagger} c_{N\sigma} + h.c.) - \bar{E}_{G,N+1}$ , with  $\bar{E}_{G,N+1}$  chosen so that the ground state energy of  $\bar{H}_{N+1}$  is zero. The Hamiltonians  $\bar{H}_N$  are diagonalized

within subspaces of well defined  $Q, N_e, S, S_z$  where  $N_e$  is the total fermion number,  $S$  the total spin and  $S_z$  the z-component of total spin. The use of these conserved quantities leads to significant reductions in the size of matrices to be diagonalized, however the dimension of  $\bar{H}_N$  grows as  $4^N$  and it is necessary to truncate the higher energy states for  $N > 7$ . Approximately 1/4 of the states generated at each iteration are retained in the calculations and this constitutes a surprisingly accurate approximation for the present model. This accuracy is evidenced by the fact that various exact relations, such as the Friedel sum rule, which relates the impurity spectral density at the Fermi level to the local level occupancy, are satisfied to a high degree of accuracy [15]. In addition, the number of states retained per iteration,  $N_{st}$ , which is a free parameter, can be varied from 250 to 2000 states without any significant change in the results presented here. This, together with the almost cut-off independent results for  $\Lambda \geq 1.5$  indicates the convergence and accuracy of the method.

## B. NRG Calculation of Auxiliary Spectral Functions

Within the framework of the NRG it is natural to represent the Green functions in an eigenbasis of the Hamiltonian. In the enlarged Hilbert space the retarded propagators for pseudo-fermions and slave-bosons are defined by

$$G_{f\sigma}(\omega + i0, T, \lambda) = \frac{1}{Z_{GC}} \sum_{Q,m,n} |M_{m,n}^f|^2 (e^{-\beta(\epsilon_n + \lambda Q)} + e^{-\beta(\epsilon_m + \lambda(Q+1))}) / (\omega + i0 - \lambda - (\epsilon_m - \epsilon_n)),$$

$$G_b(\omega + i0, T, \lambda) = \frac{1}{Z_{GC}} \sum_{Q,m,n} |M_{m,n}^b|^2 (e^{-\beta(\epsilon_n + \lambda Q)} - e^{-\beta(\epsilon_m + \lambda(Q+1))}) / (\omega + i0 - \lambda - (\epsilon_m - \epsilon_n)),$$

where, for each  $Q$ ,  $\epsilon_m, \epsilon_n$  are eigenvalues of the subspaces  $Q + 1, Q$ , where  $Z_{GC}(T, \lambda)$  is the grand-canonical partition function,

$$Z_{GC}(T, \lambda) = \sum_{Q,m} e^{-\beta(\epsilon_m + \lambda Q)} = Z_{Q=0} + e^{-\beta\lambda} Z_{Q=1} + \dots \quad (3)$$

and  $M_{m,n}^O = \langle Q + 1, m | O^\dagger | Q, n \rangle$  with  $O = f_\sigma, b$  are the many-body matrix elements for pseudo-fermions and slave-bosons, respectively. The constrained propagators are then obtained as

$$G_{f,b}(\omega + i0, T, \lambda \rightarrow \infty) = \frac{1}{Z_{Q=0}} \sum_{m,n} |M_{m,n}^{f,b}|^2 e^{-\beta\epsilon_n} / (\omega + i0 - (\epsilon_m - \epsilon_n)), \quad (4)$$

where the frequency has been shifted as  $\omega \rightarrow \omega + \lambda$ . We are interested in the following projected spectral functions (see Appendix C for details)  $A_{f,b}^+(\omega, T) = -\lim_{\lambda \rightarrow \infty} [\text{Im } G_{f,b}(\omega, T, \lambda) / \pi]$  and  $A_{f,b}^-(\omega, T) = -\lim_{\lambda \rightarrow \infty} \frac{e^{-\beta\omega}}{Z_C(T)} [\text{Im } G_{f,b}(\omega, T, \lambda) / \pi]$ ,

$$A_{f,b}^+(\omega, T) = \frac{1}{Z_{Q=0}(T)} \sum_{m,n} | \langle 1, m | O^\dagger | 0, n \rangle |^2 e^{-\beta\epsilon_{0,n}} \delta(\omega - (\epsilon_{1,m} - \epsilon_{0,n})), \quad (5)$$

$$A_{f,b}^-(\omega, T) = \frac{1}{Z_C(T) Z_{Q=0}(T)} \sum_{m,n} | \langle 1, m | O^\dagger | 0, n \rangle |^2 e^{-\beta\epsilon_{1,m}} \delta(\omega - (\epsilon_{1,m} - \epsilon_{0,n})), \quad (6)$$

In the definition of  $A_{f,b}^-$   $Z_C = Z_{Q=1}$  is introduced in order to obtain a well defined zero temperature limit<sup>1</sup>. At zero temperature the spectral functions reduce to

$$A_{f,b}^+(\omega, T = 0) = \frac{1}{Z_{Q=0}(0)} \sum_m | \langle 1, m | O^\dagger | \Phi_0 \rangle |^2 \delta(\omega + E_{Q=0}^{GS} - \epsilon_{1,m}), \quad (7)$$

$$A_{f,b}^-(\omega, T = 0) = \frac{1}{Z_C(0) Z_{Q=0}(0)} \sum_n | \langle \Phi_1 | O^\dagger | 0, n \rangle |^2 \delta(\omega + \epsilon_{0,n} - E_{Q=1}^{GS}). \quad (8)$$

Here  $|\Phi_0\rangle$  is the groundstate of the  $Q = 0$  subspace of non-interacting conduction electrons and  $|1, m\rangle$  are the excited states of the  $Q = 1$  subspace of the interacting system,  $E_{Q=0}^{GS}$  and  $\epsilon_{1,m}$  are the corresponding energy eigenvalues. The spectral functions  $A_{f,b}^+(T = 0)$  vanish identically *below* the threshold  $E_0 = E_{Q=1}^{GS} - E_{Q=0}^{GS}$ . Similarly, in the expression for  $A_{f,b}^-(T = 0)$ ,  $|\Phi_1\rangle$  is the groundstate of the interacting system ( $Q = 1$  subspace) and  $|0, n\rangle$  are the excited states of the non-interacting conduction electron system,  $E_{Q=1}^{GS}$  and  $\epsilon_{0,n}$  the corresponding energy eigenvalues. These spectral functions vanish *above* the threshold energy  $E_0$ . From (B4-B5) and (7) we see that the  $T = 0$  spectral functions  $A_{f,b}^+$  satisfy the sum rule

$$\int_{-\infty}^{+\infty} A_{f,b}^+(\omega, 0) d\omega = 1 \quad (9)$$

---

<sup>1</sup> The functions  $A_f^+$ ,  $A_b^+$  defined here correspond to the  $A$ ,  $B$  functions, respectively in Ref. [7], and similarly the functions  $A_f^-$ ,  $A_b^-$  correspond to the  $a$  and  $b$  functions.

In practice, within the NRG technique, it is the excitation energies from the respective  $Q = 0$  or  $Q = 1$  groundstates which are calculated. Hence, it is convenient to set the threshold energy,  $E_0$ , to zero. The  $T = 0$  projected auxiliary spectral functions then have divergences at zero energy. As described in Appendix D it is also possible to formulate the NCA equations of section C such that the NCA spectral functions exhibit their  $T = 0$  divergences at zero energy. This makes it easier to compare with the NRG results and in addition improves the accuracy of the NCA solution at the lowest temperatures. The reference energy scale for the physical  $d$  electron Green's function,  $G_{d\sigma}(\omega, T) = \langle\langle b^\dagger f_\sigma; b f_\sigma^\dagger \rangle\rangle_{Q=1}$ ,

$$G_{d\sigma}(\omega + i0, T) = \frac{1}{Z_C} \sum_{m,n} |M_{m,n}^d|^2 (e^{-\beta\epsilon_n} + e^{-\beta\epsilon_m}) / (\omega + i0 - (\epsilon_m - \epsilon_n)), \quad (10)$$

is independent of  $E_0$  and is set by the Fermi level  $\epsilon_F = 0$ .

The matrix elements  $M_{m,n}^{f,b}$  of the pseudo-particle operators  $f_\sigma^\dagger, b^\dagger$  in (5–6) are calculated recursively using the formulae given in Appendix A. Similar formulae apply to the matrix elements  $M_{m,n}^d$  for the physical  $d$  electron Green's function. For each iteration step, they are substituted together with the energy eigenvalues into (7–8) to give the  $T = 0$  spectral functions  $\bar{A}_{N,f,b}^\pm(\omega)$ . In principle if all states up to stage  $N$  were retained,  $H_N$  would describe excitations on all energy scales from the band edge  $D = 1$  down to the lowest energy scale present in  $H_N$ , i.e.  $\omega_N$ . Due to the elimination of higher energy states at each step, the actual range of excitations in  $H_N$  is restricted to  $\omega_N \leq \omega \leq K\omega_N$ , where  $K \approx 7$  for  $\Lambda \approx 2$  retaining 500 states per iteration. Thus at step  $N$ , the spectral functions are calculated at an excitation energy  $\omega \approx 2\omega_N$  in the above range. The delta functions in (7–8) are broadened with Gaussians of width  $\alpha_N \approx \omega_N$  appropriate to the energy level structure of  $H_N$  [15].

Finally we note that the constraint of no double occupancy,  $Q = 1$ , is implemented exactly within the NRG calculations since  $Q$  is a conserved quantum number. Appendix C describes in detail the implementation of this constraint for the conserving approximation of following section.



### C. Conserving approximation: NCA

For small hybridization  $V$  compared to the impurity level  $\epsilon_d$ , a perturbation expansion in terms of  $V$  seems reasonable. It is useful to express the auxiliary particle Green's functions for given "chemical potential"  $-\lambda$  defined in (C1) in terms of self-energies  $\Sigma_b(\omega, T, \lambda)$  and  $\Sigma_f(\omega, T, \lambda)$  as

$$G_{f\sigma}(\omega, T, \lambda) = [\omega - \lambda - \epsilon_d - \Sigma_f(\omega, T, \lambda)]^{-1} \quad (11)$$

$$G_b(\omega, T, \lambda) = [\omega - \lambda - \Sigma_b(\omega, T, \lambda)]^{-1} \quad (12)$$

where  $\omega$  takes the values of fermionic or bosonic Matsubara frequencies. The projected spectral functions are obtained by shifting the frequency  $\omega \rightarrow \omega + \lambda$  and taking the limit  $\lambda \rightarrow \infty$ , as described in Appendix C. The local Green's function of conduction electrons  $G_{c\sigma}(\omega, T, \lambda)$  is given likewise in terms of the self energy  $\Sigma_{c\sigma}(\omega, T, \lambda)$  as

$$G_{c\sigma}(\omega, T, \lambda) = [(G_{c\sigma}^0)^{-1} - \Sigma_{c\sigma}(\omega, T, \lambda)]^{-1} \quad (13)$$

where  $G_{c\sigma}^0(\omega) = \int d\epsilon N(\epsilon)/(\omega - \epsilon)$  is the local Green's function of the bare conduction band, with  $N(\epsilon)$  the density of states. There is an exact relation between the d-electron Green's function and  $\Sigma_c$ :

$$G_{d\sigma}(\omega, T, \lambda) = \frac{1}{V^2} \frac{\Sigma_{c\sigma}(\omega, T, \lambda)}{1 - \Sigma_{c\sigma}(\omega, T, \lambda) G_{c\sigma}^0(\omega)}. \quad (14)$$

Thus, the principal problem remaining in the evaluation of the theory is the proper choice of approximation in which the three self-energies are calculated. The slave-boson Hamiltonian (1) is invariant under two independent  $U(1)$  gauge transformations: (1) simultaneous transformation of the pseudo-fermion and the slave-boson operators and (2) simultaneous transformation of the pseudo-fermion and the conduction electron operators. These symmetries correspond to the conservation of the auxiliary particle number and the total number of fermions, respectively:

$$\sum_{\sigma} f_{\sigma}^{\dagger} f_{\sigma} + b^{\dagger} b = \text{const.} \quad (15)$$

$$\sum_{\sigma} f_{\sigma}^{\dagger} f_{\sigma} + \sum_{k\sigma} c_{k\sigma}^{\dagger} c_{k\sigma} = \text{const.} \quad (16)$$

The Green's functions  $G_f$ ,  $G_b$  are not invariant under local (in time) gauge transformations, but we must require  $G_d$  to be invariant. Constructing a gauge invariant approximation is, a priori, a non-trivial task, since the  $d$  electron number  $n_d$  is not a conserved quantity. Yet, it may be shown that a gauge invariant approximation obeying both conservation laws (15), (16) is constructed by deriving all three self-energies from one generating functional  $\Phi$ :  $\Sigma_{f\sigma} = \delta\Phi/\delta G_{f\sigma}$ ,  $\Sigma_b = \delta\Phi/\delta G_b$ ,  $\Sigma_{c\sigma} = \delta\Phi/\delta G_{c\sigma}$ . Eq. (14) then provides the rule for a gauge invariant approximation for  $G_d$ . The functional  $\Phi$  is given in terms of closed skeleton diagrams with suitable combinatorial factors. The lowest order contribution to  $\Phi$  is of second order in  $V$ ,  $\Phi = -V^2 \frac{1}{\beta} \sum_{\omega} \sum_{\epsilon} G_{f\sigma}(\omega) G_{c\sigma}(\epsilon) G_b(\omega - \epsilon)$  (Fig. 1 a). Functional differentiation yields the self-energies

$$\Sigma_{f\sigma}(\omega) = -V^2 \frac{1}{\beta} \sum_{\epsilon} G_{c\sigma}(\epsilon) G_b(\omega - \epsilon) \quad (17)$$

$$\Sigma_b(\Omega) = V^2 \frac{1}{\beta} \sum_{\epsilon} G_{f\sigma}(\Omega + \epsilon) G_{c\sigma}(\epsilon) \quad (18)$$

$$\Sigma_{c\sigma}(\omega) = -V^2 \frac{1}{\beta} \sum_{\epsilon} G_{f\sigma}(\epsilon) G_b(\epsilon - \omega). \quad (19)$$

After the transformation  $\omega \rightarrow \omega + \lambda$ ,  $\lambda \rightarrow \infty$ , one finds explicitly

$$\Sigma_{f\sigma}(\omega, T) = V^2 \sum_k (1 - f(\epsilon_k)) G_b(\omega - \epsilon_k) \quad (20)$$

$$\Sigma_b(\omega, T) = V^2 \sum_{k,\sigma} f(\epsilon_k) G_{f\sigma}(\omega + \epsilon_k), \quad (21)$$

$$\Sigma_{c\sigma}(\omega, T, \lambda \rightarrow \infty) = V^2 e^{-\beta\lambda} \int d\epsilon e^{-\beta\epsilon} [G_{f\sigma}(\epsilon + \omega) A_b^+(\epsilon) - A_f^+(\epsilon) G_b(\epsilon - \omega)] \quad (22)$$

and  $G_{f\sigma}(\omega)^{-1} = \omega - \epsilon_d - \Sigma_{f\sigma}(\omega)$ ,  $G_b(\omega)^{-1} = \omega - \Sigma_b(\omega)$ , where  $f(\epsilon_k)$  is the Fermi function. The physical d-electron Green's function is obtained from the limiting procedure  $G_{d\sigma}(\omega, T) = \lim_{\lambda \rightarrow \infty} e^{\beta\lambda} G_{d\sigma}(\omega, T, \lambda)$  (compare Appendix C). As  $\Sigma_{c\sigma}(\omega, T, \lambda) \sim e^{-\beta\lambda}$  for  $\lambda \rightarrow \infty$ , the self-energy corrections to  $G_c$  and to the denominator of  $G_d$  vanish, and

$$G_{d\sigma}(\omega, T) = \frac{1}{V^2} \lim_{\lambda \rightarrow \infty} e^{\beta\lambda} \Sigma_{c\sigma}(\omega, T, \lambda). \quad (23)$$

The impurity spectral density follows as,

$$\begin{aligned}
\rho_d^{NCA}(\omega, T) &= -\frac{1}{\pi} \text{Im} G_{d\sigma}(\omega + i0, T) \\
&= \int_{-\infty}^{+\infty} d\epsilon [A_f^+(\epsilon + \omega, T)A_b^-(\epsilon, T) + A_f^-(\epsilon, T)A_b^+(\epsilon - \omega, T)], \tag{24}
\end{aligned}$$

which at  $T = 0$  reduces to,

$$\begin{aligned}
\rho_d^{NCA}(\omega, T = 0) &= \Theta(\omega) \int_{E_0 - \omega}^{E_0} d\epsilon A_f^+(\epsilon + \omega, T = 0)A_b^-(\epsilon, T = 0) \\
&\quad + \Theta(-\omega) \int_{E_0 + \omega}^{E_0} d\epsilon A_f^-(\epsilon, T = 0)A_b^+(\epsilon - \omega, T = 0). \tag{25}
\end{aligned}$$

The above approximation is known as the ‘‘non-crossing approximation’’ (NCA) because it does not include any diagrammatical contributions with crossed conduction electron lines [10].

In general the impurity electron Green’s function may be expressed with the help of a vertex function  $\Lambda(\epsilon, \omega)$  as (Fig. 1 b)

$$G_{d\sigma}(\omega) = -\lim_{\lambda \rightarrow \infty} e^{\beta\lambda} \sum_{\epsilon} G_{f\sigma}(\epsilon)G_b(\epsilon - \omega)\Lambda(\epsilon, \omega) \tag{26}$$

As shown below, there is reason to expect that the vertex function  $\Lambda$  plays an important role.

### III. RESULTS

The NRG calculations were performed for  $\Lambda = 2$ , keeping 250 states per iteration for each subspace ( $Q = 0, 1$ ). The hybridization strength  $\Delta = \pi V^2 \rho(\epsilon_F) = \pi V^2/2D$  was chosen to be  $0.01D$  with the half-bandwidth  $D = 1$ . Several values of the local level position  $\epsilon_d$  were chosen in order to characterize the behaviour of the spectral densities in the various regimes. The NRG spectral functions were evaluated at  $T = 0$  and the NCA spectral functions were evaluated following appendix D for the same set of parameters and for temperatures down to  $T = 10^{-6}D \ll T_0$ , where  $T_0$  is the low energy scale of the model. This was sufficiently low to allow comparison with the  $T = 0$  NRG results over most of the interesting energy range. We define  $T_0$  to be the Kondo temperature,

$$k_B T_K = D \sqrt{\frac{\Delta}{D}} e^{-\pi \epsilon_d / 2\Delta} \quad (27)$$

in the Kondo regime  $\epsilon_d/\Delta \leq -2$ ,  $\Delta$  in the mixed valent regime  $|\epsilon_d/\Delta| \leq 1$  and  $\epsilon_d$  in the empty orbital regime  $\epsilon_d/\Delta \gg 1$ .

### A. Threshold behaviour of the NRG auxiliary spectral functions

The  $T = 0$  auxiliary spectral functions diverge at the threshold  $E_0$  as shown in Fig. (2–4). This behaviour may be understood as a result of the orthogonality catastrophe theorem [16]. To see this more clearly we re-formulate the spectral densities in (7–8) in the following way,

$$A_{f,b}^+(\omega, T = 0) = \frac{1}{Z_{Q=0}} \sum_m |\langle 1, m | \tilde{\Phi}_0 \rangle|^2 \delta(\omega - \epsilon_{1,m}), \quad (28)$$

$$A_{f,b}^-(\omega, T = 0) = \frac{1}{Z_{Q=0}} \sum_n |\langle \tilde{\Phi}_1 | 0, n \rangle|^2 \delta(\omega + \epsilon_{0,n}). \quad (29)$$

In the above,  $|\tilde{\Phi}_0 \rangle = O^\dagger |\Phi_0 \rangle$ , with  $O = f_\sigma, b$ , represents the non-interacting ( $U = 0$ ) groundstate with 1 ( $O = f_\sigma^\dagger$ ) or 0 ( $O = b^\dagger$ ) local electrons present. Similarly,  $|\tilde{\Phi}_1 \rangle = O |\Phi_1 \rangle$ , with  $O = f_\sigma, b$ , represents the interacting ( $U = \infty$ ) groundstate with 1 ( $O = f_\sigma^\dagger$ ) or 0 ( $O = b^\dagger$ ) local electrons present. In this formulation, we see that  $A_{f,b}^+$  measures the overlap density between the groundstate of the non-interacting ( $U = 0$ ) band electrons with 0 or 1 local electrons present with the excited states of the interacting  $U = \infty$  Hamiltonian. Similarly,  $A_{f,b}^-$  measures the overlap density between the groundstate of the interacting  $U = \infty$  Hamiltonian with 0 or 1 local electrons present and the excited states of the non-interacting band electrons. This interpretation is identical to that for the core level spectral functions in the X-ray problem. The analogy is useful but requires care since the matrix elements in (5–6) are no longer between two non-interacting systems as in the X-ray problem. This leads in particular to a new energy scale,  $T_0$ , for the onset of the asymptotic power law behaviour, which is  $T_K$ ,  $\Delta$  or  $\epsilon_d$  in the Kondo, mixed valent and empty orbital regimes, respectively. We find that it is only in the Fermi liquid regime,  $|\omega - E_0| \ll T_0$ , that the

power law behaviour is well characterized. The approach to this asymptotic power law is faster for the boson spectral functions than for the fermion spectral functions in all cases. We note that within the NCA, the approach to the threshold behaviour with  $n_d$  independent exponents  $\alpha_f = 1/3$  and  $\alpha_b = 2/3$  is also only asymptotic and requires in particular going down to temperatures  $T < 10^{-2}T_0$  in order to see these exponents.

The threshold exponents for the slave-boson and pseudo-fermion spectral functions were extracted by numerically differentiating the spectral functions. Typically, well defined exponents can be extracted only for energy scales  $|\omega - E_0| < 10^{-2}T_0$ . The exponents are shown in Fig. (5) and Table I as a function of  $n_d$ , the local level occupancy at  $T = 0$ . The latter, shown in Fig. (6), was calculated by evaluating  $n_d(T)$  from the partition function at a sequence of decreasing temperatures  $T_N \sim \Lambda^{-(N-1)/2}$  and then taking the limit  $T \rightarrow 0$ .

Remarkably, the threshold exponents turn out to be the usual photoemission and absorption exponents for the X-ray problem and are given in terms of the conduction electron phase-shift at the Fermi level [12],  $\delta_\sigma = \delta_\sigma(\epsilon_F)$ , by

$$\alpha_f = n_d - \frac{n_d^2}{2} = 2\frac{\delta_\sigma}{\pi} - \sum_\sigma \left(\frac{\delta_\sigma}{\pi}\right)^2 \quad (30)$$

$$\alpha_b = 1 - \frac{n_d^2}{2} = 1 - \sum_\sigma \left(\frac{\delta_\sigma}{\pi}\right)^2 \quad (31)$$

where the last equations on the RHS of (30–31) follow from the Friedel sum rule,  $\delta_\sigma = \pi n_d/2$ . These results are clearly illustrated in Fig. (5) where the functions  $n_d - n_d^2/2$  and  $1 - n_d^2/2$  are plotted against  $n_d$  together with the exponents  $\alpha_{f,b}$  deduced from the spectral functions. The exponents  $\alpha_{f,b}$  agree with the RHS of (30–31) to 3 significant figures in nearly all cases and are the same below and above the threshold,

$$A_{f,b}^\pm = a_{f,b}^\pm |\omega - E_0|^{-\alpha_{f,b}} \quad (32)$$

A qualitative argument based on charge neutrality considerations has been given for the above form of the exponents [12]. We note that the same functional form of the exponents on the phase shift (30–31) is also found in the spinless model with constraint [13] in agreement with exact analytic results [19]. The single phase shift in this case is given by  $\delta = \pi n_d$

. An  $n_d$  dependent exponent was also found by Read in considering how Gaussian and higher order corrections restore the gauge symmetry broken by the slave-boson mean field theory [18]. Generalizing the above threshold exponents to the  $N$ -fold degenerate model we have  $\alpha_f = 2\delta_m/\pi - \sum_m(\delta_m/\pi)^2 = 2n_d/N - n_d^2/N$  and  $\alpha_b = 1 - \sum_m(\delta_m/\pi)^2 = 1 - n_d^2/N$  where  $m$  labels the scattering channels. The same exponents were found for the  $N$ -fold degenerate Anderson impurity model in perturbative calculations to order  $V^4$  [19] adding to the plausibility of the above generalization. The above conjecture for  $\alpha_{f,b}$  is in disagreement with recent results obtained in the limit  $n_d \rightarrow 1$  and in the large  $N$  expansion including order  $1/N^2$  [20],  $\tilde{\alpha}_f = \frac{1-\frac{1}{N^2}}{N+1-\frac{1}{N^2}}$ ,  $\tilde{\alpha}_b = \frac{N-\frac{2}{N^2}}{N+1-\frac{1}{N^2}}$ . These results were obtained using a perturbative renormalization group technique, which we do not expect to be as accurate as the non-perturbative numerical scheme used here. We see from our results, generalized to arbitrary  $N$ , that the NCA exponents  $1/(N+1) = 1/N + O(1/N^2)$  and  $N/(N+1) = 1 - 1/N + O(1/N^2)$  are correct only in the limit  $n_d \rightarrow 1$  and  $N \rightarrow \infty$  (or in the trivial limit  $n_d \rightarrow 0$ ). Away from this limit, vertex corrections in the auxiliary Green's functions, absent in the NCA, are therefore important in determining the correct threshold exponents. The expressions for the threshold exponents of auxiliary particle propagators in terms of X-ray photoemission exponents appears to be a general property of several impurity models exhibiting Fermi liquid fixed points.

## B. NRG auxiliary spectral functions at higher energies

At higher frequencies the following features are observed in the  $T = 0$  spectral functions. In the Kondo regime, Fig. (2), there is a peak in the slave-boson spectral function  $A_b^+$  at  $\omega = |\epsilon_d|$  and a much less pronounced feature in the corresponding pseudo-fermion spectral function  $A_f^+$ . As  $\epsilon_d$  is raised through the Fermi level from below the peak in  $A_b^+$  at  $\omega = |\epsilon_d|$  becomes less pronounced and almost disappears in the mixed valent  $\epsilon_d/\Delta \sim 0$ , Fig. (3), and empty orbital regimes  $\epsilon_d/\Delta > 1$  Fig. (4). In addition, its position is renormalized above the bare value  $|\epsilon_d|$ . At the same time the small feature at positive energies in the

pseudo-fermion spectral function  $A_f^+$  develops into a well defined peak in the mixed valent and empty orbital regimes. The “-” spectral functions  $A_{f,b}^-(\omega, T = 0)$  exhibit monotonic behaviour for all parameter regimes.

### C. Comparison of NRG and NCA auxiliary spectral functions

In comparing NRG and NCA spectral functions, three energy regimes should be distinguished:

- (I) asymptotically low energy regime,  $|\omega - E_0|/T_0 \ll 1$ ,
- (II) crossover regime,  $|\omega - E_0|/T_0 \sim 1$ ,
- (III) high energy regime,  $|\omega - E_0|/T_0 \gg 1$ .

The energy range (I) corresponds to that discussed in the section on threshold exponents. Here we discuss the energy ranges between (I) and (II), and between (II) and (III). In Fig. (7–9) the same qualitative trends described in the previous section for the NRG auxiliary spectral functions can be seen in the corresponding NCA solutions. The NCA results for a finite but very low temperature  $T = 10^{-6}D$  are compared to the corresponding  $T = 0$  NRG results. Surprisingly good quantitative agreement is seen in the slave-boson spectral function  $A_b^+$  above the threshold down to energy scales well below  $T_0$  in all regimes. The agreement is particularly good in the Kondo regime for  $-4 \leq \epsilon_d/\Delta \leq -2$ , where it extends down to  $10^{-2}T_0$  (e.g., Fig. 7a). The spectral function  $A_b^-$  below the threshold also shows good agreement with the NRG result in the Kondo regime with decreasing agreement in the mixed valent  $\epsilon_d/\Delta \sim 0$  and empty orbital regimes  $\epsilon_d/\Delta \gg 1$ . Turning now to the pseudo-fermion spectral functions we see that there is again good quantitative agreement between NCA and NRG for  $A_f^+$  above the threshold and for all energy scales down to  $T_0$ . This is true in all regimes. Below the threshold the agreement for the  $A_f^-$  spectral function even extends to well below  $T_0$ , except in the Kondo regime for  $\epsilon_d/\Delta \leq -4$  where we could not obtain quantitative agreement except in the region  $10^{-1} \leq \omega \leq 10^1$ . From

these comparisons we see that the most serious differences, as far as low energy behaviour is concerned, between the NCA and NRG auxiliary spectral functions are in  $A_f^+$  for  $\omega < T_0$  in the Kondo case and in  $A_b^-$  in the mixed valent and empty orbital cases. The latter we attribute to the inaccuracy of the NCA in the energy range between (I) and (II) in the mixed valent and empty orbital regimes to be described further in the section on impurity spectral densities. A more interesting discrepancy which arises from these comparisons is the former. The functions  $A_{f,b}^+$  in NCA are related by self-consistency equations (20–21) derived by second order perturbation theory in  $V$ . As pointed out in [22], coherent spin flip processes considered to be responsible for the Kondo resonance are not included in the NCA. There are reasons to expect that the self-consistent T-matrix approximation proposed in [22] will capture the essential contributions. Recent calculations within the conserving self-consistent T-matrix approximation indicate that such improvements do indeed arise [23].

A different extension of NCA, called “post-NCA” has been proposed recently on the basis of a  $\frac{1}{N}$  expansion of the N-orbital model [21]. It represents a self-consistent scheme including vertex renormalizations, which is exact to order  $1/N^2$ .

#### D. Comparison of NRG and NCA impurity spectral functions

In the previous section we noted that the NCA auxiliary spectral functions were surprisingly close to the NRG ones for energies down to at least  $\omega = T_0$  and typically they were even quantitatively accurate down to  $\omega \ll T_0$ . Improvements are primarily important in the auxiliary spectral functions in two areas, to restore the correct behaviour of the pseudo-fermion spectral function  $A_f^+$  below  $T_0$  and to recover the exact threshold exponents given by the NRG. We now turn to the comparisons for the impurity spectral function and discuss the role of vertex corrections on the dynamics of the physical electrons. The impurity spectral densities are shown in Fig. (10–12) where in addition to the NCA,  $\rho_d^{NCA}(\omega)$ , and NRG spectral functions,  $\rho_d^{NRG}(\omega)$ , we also show the impurity spectral function,  $\rho_d^{NRG-}$ , obtained



by convoluting the NRG auxiliary spectral functions as in (26) but without the vertex part, i.e.

$$\rho_d^{NRG-}(\omega, T) = \int_{-\infty}^{+\infty} d\epsilon [A_f^+(\epsilon + \omega, T)A_b^-(\epsilon, T) + A_f^-(\epsilon, T)A_b^+(\epsilon - \omega, T)]. \quad (33)$$

In the Kondo regime (Fig. 10 a-c), the impurity spectral density shows two peaks, a charge fluctuation peak close to the local level position  $\epsilon_d$ , and a many-body Kondo resonance at the Fermi level. The charge fluctuation peak is broader in the NRG case, a result of using a logarithmic discretization for the conduction band which leads to lower resolution at higher energies. This is not a fundamental problem with the NRG, and the resolution of the method at higher energies can be improved by reducing the discretization parameter  $\Lambda$  for the relevant iterations covering the high energy scales. We have explicitly checked that the width and height of the many-body resonance at the Fermi level, where the NRG gives the highest resolution, are unaffected by the broadening used to smooth the delta functions in the discrete spectra (unless the broadening is made too small which will result in uneven spectra). From Fig. 10b-c we see that the NCA gives a Kondo resonance which is too broad and too high on the BIS ( $\omega > 0$ ) side for energies below  $\sim 5T_0$ . On the PES side ( $\omega < 0$ ), i.e. for  $\omega < 0$ , the agreement with the NRG is better.

The disagreement between the NCA and NRG impurity spectral function for energies below  $5T_0$  is due primarily to the absence of the vertex part in the convolution formula for the NCA impurity spectral density (24). This is seen from the good agreement between  $\rho_d^{NRG-}$  and  $\rho_d^{NCA}$  in the range  $T_0 \leq \omega \leq 5T_0$  which indicates that the NCA auxiliary spectral functions are sufficiently accurate in this range and that *therefore the difference between  $\rho_d^{NRG}$  and  $\rho_d^{NCA}$  must be mainly due to the neglect of the vertex part in (24)*. Similar comparisons for the other Kondo cases  $\epsilon_d/\Delta = -5, -3$  support the same conclusion. In Table I we also list  $\rho_d^{NRG}(\omega = 0)$  and  $\rho_d^{NCA}(\omega = 0, T = 10^{-6}D)$  together with the respective relative deviations from the exact Friedel sum rule result,  $\rho_{d\sigma}(\omega = 0) = \sin^2(\pi n_d/2)/\pi\Delta$ . The NCA result in the Kondo regime appears reasonable because the singular behaviour of the impurity spectral density at  $T = 0$  [11] is removed by our small finite temperature

$T = 10^{-6}D$ . The exact NCA result for  $\rho_d^{NCA}(\omega = 0, T = 0)$  is actually much worse [11].

We also show results for the mixed valent, Fig. (11), and empty orbital regimes, Fig. (12). There is good agreement between  $\rho_d^{NRG}$ ,  $\rho_d^{NRG-}$  and  $\rho_d^{NCA}$  for the high energy parts of the renormalized resonant level  $\omega \geq T_0$ , but the incorrect low energy behaviour of the NCA result for  $A_b^+$  in the above regimes and the neglect of the vertex part in (24) and (33) makes both  $\rho_d^{NCA}$  and  $\rho_d^{NRG-}$  deviate from the exact NRG result at low energies. The resonant level is approximately a Lorentzian of width  $\Delta$ , and the small asymmetric broadening in the NRG curves is due to the logarithmic discretization. An improved description of high energies could be obtained in both NRG and NCA, if required. Within NRG it is possible to focus on high energies explicitly by using a smaller discretization parameter,  $\Lambda$ , for the first few iterations. Within NCA higher energies are easily resolved by using a finer grid to solve the integral equations at these energies.

Having discussed the effect of vertex corrections on the impurity spectral function at intermediate  $\omega \sim T_0$  and higher energies  $\omega > T_0$  in the different parameter regimes, we now discuss the limit  $\omega \ll T_0$ . In this limit, evaluating the impurity spectral density, without vertex corrections, i.e. for  $\Lambda = 1$ , using (30–32) in (26) gives

$$\rho'_{d\sigma}(\omega \rightarrow 0^+) = a_f^+ a_b^- \omega^{1-\alpha_f-\alpha_b} B(1-\alpha_f, 1+\alpha_b) \sim |\omega|^{-n_d(1-n_d)}. \quad (34)$$

where  $B$  is the Beta function. The exact result at  $\omega = 0$  is given by the Friedel sum rule,  $\rho_{d\sigma}(\omega = 0) = \sin^2(\pi n_d/2)/\pi\Delta$ , so we conclude that the vertex corrections neglected in (34) are singular at low energies, i.e. close to the threshold, and lead to a singularity in  $\rho_{d\sigma}$  at the Fermi level which cancels that in (34). Similar vertex corrections appear in the calculation of other physical quantities such as the dynamic spin susceptibility.

#### IV. DISCUSSION AND CONCLUSIONS

In this paper we have made a comparison of the spectral functions of the  $U = \infty$  Anderson model as calculated within the simplest self-consistent conserving approximation, the NCA,

and within the NRG. At high energies  $\omega \gg T_0$  we found good quantitative agreement for the auxiliary and physical spectral functions calculated within the two methods in all parameter regimes. Some small discrepancies in the shape of high energy peaks could be attributed to the logarithmic discretization used in the NRG which tends to give lower resolution and slight asymmetries to high energy peaks. At lower energies we found good quantitative agreement for both slave-boson and pseudo-fermion spectral functions down to at least  $T_0$ . In the Kondo regime the agreement between the NCA and NRG slave-boson spectral function  $A_b^+$  extended to well below the low energy scale  $T_0 = T_K$ . Despite the accuracy of the NCA auxiliary spectral functions down to  $T_K$  we noted that the impurity spectral density deviated from the essentially exact NRG result on energy scales up to  $5T_K$ . The source of this discrepancy was traced directly to the lack of the vertex part in the NCA expression for the impurity spectral density, thus showing that vertex corrections are required for the physical Green's functions even when the auxiliary particle dynamics appears to be correctly described within the NCA (for energies down to  $T_0$ ). In the Fermi liquid regime  $\omega \ll T_0$ , the NCA gives results for the impurity spectral density in disagreement with exact results from Fermi liquid theory. It also gives the incorrect threshold exponents  $\alpha_{f,b}$  for the auxiliary particle Green's functions. We emphasize, however, that although vertex corrections restore the Fermi liquid behaviour in the physical spectral functions and the correct low energy asymptotic behaviour of the auxiliary particle Green's functions, our results show that they are also needed for a correct description of the physical Green's functions at much higher energies  $\omega \sim T_0$ . This is the main conclusion of the comparisons we made.

We are in the process of including vertex corrections within a self-consistent theory [22], thus going beyond the lowest order conserving approximation. The availability of accurate results for dynamic properties via the NRG for impurity models makes the latter a natural testing ground for developing such approximation schemes. These schemes could then be extended to study lattice models of strongly correlated electrons, for which, at present, numerical renormalization group methods are not as well developed as for impurity models.

## ACKNOWLEDGMENTS

We are grateful to K.A. Muttalib and P. Hirschfeld for useful discussions concerning self-consistent conserving approximations. This work was supported by E.U. grant no. ERBCHRX CT93 0115 (TAC), the Alexander von Humboldt Foundation (JK) and the Deutsche Forschungsgemeinschaft (PW,TAC).

## APPENDIX A: MATRIX ELEMENTS FOR AUXILIARY PARTICLE OPERATORS

In this appendix we give the expressions for the matrix elements of the auxiliary particle operators, required for the calculation of the spectral functions. The states,  $|Q, N_e, S, S_z, r \rangle_N$ , of the Hamiltonian  $H_N$  (which includes the orbitals  $f_\sigma, c_{0\sigma}, \dots, c_{N\sigma}$ ) are labeled by the quantum numbers  $Q, N_e, S, S_z$  and an index  $r$ , where  $Q = \sum_\sigma f_\sigma^\dagger f_\sigma + b^\dagger b$  is the number of auxiliary particles,  $N_e$  is the total number of electrons,  $S$  the total spin and  $S_z$  the z-component of the total spin and the index  $r$  distinguishes states with the same conserved quantum numbers. A product basis set  $|Q, N_e, S, S_z, ri \rangle_N$  for the subspace  $(Q, N_e, S, S_z)$  of  $H_N$  in terms of eigenstates of  $H_{N-1}$  and states  $|0 \rangle, |\uparrow \rangle, |\downarrow \rangle, |\uparrow\downarrow \rangle$  of the orbital  $c_{N\sigma}$  is defined by

$$|Q, N_e, S, S_z, r, 1 \rangle_N = |Q, N_e, S, S_z, r \rangle_{N-1} |0 \rangle, \quad (\text{A1})$$

$$\begin{aligned} |Q, N_e, S, S_z, r, 2 \rangle_N &= \sqrt{\frac{S + S_z}{2S}} |Q, N_e - 1, S - \frac{1}{2}, S_z - \frac{1}{2}, r \rangle_{N-1} |\uparrow \rangle \\ &+ \sqrt{\frac{S - S_z}{2S}} |Q, N_e - 1, S - \frac{1}{2}, S_z + \frac{1}{2}, r \rangle_{N-1} |\downarrow \rangle, \end{aligned} \quad (\text{A2})$$

$$\begin{aligned} |Q, N_e, S, S_z, r, 3 \rangle_N &= -\sqrt{\frac{S - S_z + 1}{2S + 2}} |Q, N_e - 1, S + \frac{1}{2}, S_z - \frac{1}{2}, r \rangle_{N-1} |\uparrow \rangle \\ &+ \sqrt{\frac{S + S_z + 1}{2S + 2}} |Q, N_e - 1, S + \frac{1}{2}, S_z + \frac{1}{2}, r \rangle_{N-1} |\downarrow \rangle, \end{aligned} \quad (\text{A3})$$

$$|Q, N_e, S, S_z, r, 4 \rangle_N = |Q, N_e - 2, S, S_z, r \rangle_{N-1} |\uparrow\downarrow \rangle \quad (\text{A4})$$

The reduced matrix elements  ${}_N \langle Q, N_e, S, r || f^\dagger || Q - 1, N_e - 1, S \pm 1/2, s \rangle_N$  and  ${}_N \langle Q, N_e, S, r || b^\dagger || Q - 1, N_e, S, s \rangle_N$  are calculated recursively following the recursive calculation

of the matrix elements  ${}_N \langle Q, N_e, S, r | c_N^\dagger | Q, N_e - 1, S \pm 1/2, s \rangle_N$  required for setting up the Hamiltonian  $H_N$ . Details of the latter can be found in [14]. We follow the notation of [14] and denote by  $U_{Q,N_e,S}^N(r_i, p), p = 1, \dots, R_{Q,N_e,S}^N$  the matrix of eigenvectors of the subspace  $(Q, N_e S, S_z)$  of  $H_N$  where  $R_{Q,N_e,S}^N$  is the dimensionality of this subspace and  $r$  and  $i = 1, \dots, 4$  label the product state basis which is related to the diagonal basis by the unitary transformation

$$|Q, N_e, S, S_z, p \rangle_N = \sum_{r,i} U_{Q,N_e,S}(p, ri) |r \rangle_{N-1} |i \rangle \quad (\text{A5})$$

with  $|r \rangle_{N-1} |i \rangle$  denoting one of the four product states (A1–A4) defined above. Defining,

$$M_{Q,N_e,S}^{f\pm,N}(r, r') \equiv {}_N \langle Q, N_e, S, r | f^\dagger | Q - 1, N_e - 1, S \pm \frac{1}{2}, r' \rangle_N \quad (\text{A6})$$

$$M_{Q,N_e,S}^{b,N}(r, r') \equiv {}_N \langle Q, N_e, S, r | b^\dagger | Q - 1, N_e, S, r' \rangle_N, \quad (\text{A7})$$

and using the unitary transformation (A5) we have,

$$\begin{aligned} M_{Q,N_e,S}^{f\pm,N}(p, q) &\equiv {}_N \langle Q, N_e, S, p | f^\dagger | Q - 1, N_e - 1, S \pm \frac{1}{2}, q \rangle_N \\ &= \sum_{ri,r'i'} U_{Q,N_e,S}^N(p, ri) U_{Q-1,N_e-1,S\pm\frac{1}{2}}^N(q, r'i') \\ &\quad \times {}_{N-1} \langle Q, N_e, S, ri | f^\dagger | Q - 1, N_e - 1, S \pm \frac{1}{2}, r'i' \rangle_{N-1} \end{aligned} \quad (\text{A8})$$

$$\begin{aligned} M_{Q,N_e,S}^{b,N}(p, q) &\equiv {}_N \langle Q, N_e, S, p | b^\dagger | Q - 1, N_e, S, q \rangle_N \\ &= \sum_{ri,r'i'} U_{Q,N_e,S}^N(p, ri) U_{Q-1,N_e,S}^N(q, r'i') \\ &\quad \times {}_{N-1} \langle Q, N_e, S, ri | b^\dagger | Q - 1, N_e, S, r'i' \rangle_{N-1}. \end{aligned} \quad (\text{A9})$$

Evaluating these using the expressions (A1–A4) gives an expression relating the matrix elements at iteration  $N$  to those at iteration  $N - 1$ ,

$$\begin{aligned} M_{Q,N_e,S}^{f\pm,N}(p, q) &= C_{11}^\pm \sum_{rr'} U_{Q,N_e,S}^N(p, r1) U_{Q-1,N_e-1,S\pm\frac{1}{2}}^N(q, r'1) M_{Q,N_e,S}^{f\pm,N-1}(r, r') \\ &\quad + C_{22}^\pm \sum_{rr'} U_{Q,N_e,S}^N(p, r2) U_{Q-1,N_e-1,S\pm\frac{1}{2}}^N(q, r'2) M_{Q,N_e-1,S-\frac{1}{2}}^{f\pm,N-1}(r, r') \\ &\quad + C_{33}^\pm \sum_{rr'} U_{Q,N_e,S}^N(p, r3) U_{Q-1,N_e-1,S\pm\frac{1}{2}}^N(q, r'3) M_{Q,N_e-1,S+\frac{1}{2}}^{f\pm,N-1}(r, r') \\ &\quad + C_{44}^\pm \sum_{rr'} U_{Q,N_e,S}^N(p, r4) U_{Q-1,N_e-1,S\pm\frac{1}{2}}^N(q, r'4) M_{Q,N_e-2,S}^{f\pm,N-1}(r, r') \end{aligned}$$

$$\begin{aligned}
& + C_{23}^{\pm} \sum_{rr'} U_{Q,N_e S}^N(p, r2) U_{Q-1, N_e-1, S \pm \frac{1}{2}}^N(q, r'3) M_{Q, N_e-1, S \pm \frac{1}{2}}^{f \mp, N-1}(r, r') \\
& + C_{32}^{\pm} \sum_{rr'} U_{Q, N_e S}^N(p, r3) U_{Q-1, N_e-1, S \pm \frac{1}{2}}^N(q, r'2) M_{Q, N_e-1, S \pm \frac{1}{2}}^{f \mp, N-1}(r, r'),
\end{aligned}$$

and,

$$\begin{aligned}
M_{Q, N_e, S}^{b, N}(p, q) & = \sum_{rr'} U_{Q, N_e S}^N(p, r1) U_{Q-1, N_e, S}^N(q, r'1) M_{Q, N_e, S}^{b, N-1}(r, r') \\
& + \sum_{rr'} U_{Q, N_e S}^N(p, r2) U_{Q-1, N_e, S}^N(q, r'2) M_{Q, N_e, S - \frac{1}{2}}^{b, N-1}(r, r') \\
& + \sum_{rr'} U_{Q, N_e S}^N(p, r3) U_{Q-1, N_e, S}^N(q, r'3) M_{Q, N_e-1, S + \frac{1}{2}}^{b, N-1}(r, r') \\
& + \sum_{rr'} U_{Q, N_e S}^N(p, r4) U_{Q-1, N_e, S}^N(q, r'4) M_{Q, N_e-2, S}^{b, N-1}(r, r'),
\end{aligned}$$

where the coefficients  $C_{ii'}^{\pm}$  are given in Table II.

## APPENDIX B: ERRORS AND SUM RULES

In this appendix we outline some of the checks carried out to ensure the correctness of the numerical renormalization group programs. The eigenvectors and eigenvalues of  $H_0$  can be calculated analytically and these can then be used to set up the matrices for  $N = 1$ . The latter have been compared with those generated by the computer programs for  $N = 1$  and found to be identical. We have also checked the recursive evaluation of the matrix elements,  $\langle r | f_{\sigma}^{\dagger} | s \rangle$ ,  $\langle r | b^{\dagger} | s \rangle$  and  $\langle r | c_{N\sigma}^{\dagger} | s \rangle$  by making use of the commutation relations for the creation and annihilation operators appearing in the Hamiltonian (1),

$$f_{\sigma} f_{\sigma}^{\dagger} + f_{\sigma}^{\dagger} f_{\sigma} = 1, \quad (\text{B1})$$

$$b_{\sigma} b_{\sigma}^{\dagger} - b_{\sigma}^{\dagger} b_{\sigma} = 1, \quad (\text{B2})$$

$$c_{N\sigma} c_{N\sigma}^{\dagger} + c_{N\sigma}^{\dagger} c_{N\sigma} = 1. \quad (\text{B3})$$

For any state  $|Q, N_e, S, S_z, k \rangle_N$  in the Hilbert space of  $H_N$ , the completeness relation  $\sum_r |r \rangle \langle r| = 1$  together with (B1–B3) yields,

$$1 = \sum_{k'} | \langle Q, N_e, S, k | f^{\dagger} | Q-1, N_e-1, S - \frac{1}{2}, k' \rangle |^2$$

$$\begin{aligned}
& + \frac{1}{2S+2} \sum_{k'} | \langle Q, N_e, S, k' | f^\dagger | Q-1, N_e-1, S+\frac{1}{2}, k' \rangle |^2 \\
& + \sum_{k'} | \langle Q+1, N_e+1, S+\frac{1}{2}, k' | f^\dagger | Q, N_e, S, k \rangle |^2,
\end{aligned} \tag{B4}$$

$$\begin{aligned}
1 & = \sum_{k'} | \langle Q+1, N_e, S, k' | b^\dagger | Q, N_e, S, k \rangle |^2 \\
& - \sum_{k'} | \langle Q, N_e, S, k | b^\dagger | Q-1, N_e, S, k' \rangle |^2,
\end{aligned} \tag{B5}$$

$$\begin{aligned}
1 & = \sum_{k'} | \langle Q, N_e, S, k | c_N^\dagger | Q, N_e-1, S-\frac{1}{2}, k' \rangle |^2 \\
& + \frac{1}{2S+2} \sum_{k'} | \langle Q, N_e, S, k | c_N^\dagger | Q, N_e-1, S+\frac{1}{2}, k' \rangle |^2 \\
& + \sum_{k'} | \langle Q, N_e+1, S+\frac{1}{2}, k' | c_N^\dagger | Q, N_e, S, k \rangle |^2.
\end{aligned} \tag{B6}$$

In the calculations we verified that these relations were satisfied to within rounding errors for each state  $|Q, N_e, S, k \rangle_N$  in  $H_N$  for  $N = 0, 1, \dots, 4$ , when all states are retained. This gives a reliable test of the formulae in Appendix A and on the routines for the recursive evaluation of the matrix elements. We note that once higher energy states start being eliminated, typically for  $N > 4$ , the LHS of the above expressions will be less than unity due to the missing states. The sum rule (B6) also provides a check on the construction of the Hamiltonian  $H_N$ , since the latter depends on the matrix elements  $\langle Q=1, N_e+1, S \pm \frac{1}{2}, k' | c_N^\dagger | Q=1, N_e, S, k \rangle$  [14]. The above tests on all quantities appearing in the iterative procedure for the first few iterations virtually eliminates the possibility of errors.

### APPENDIX C: EXACT PROJECTION ONTO THE PHYSICAL SUBSPACE

In order to effect the constraint of the dynamics to the physical Hilbert subspace it is convenient to add the term  $\lambda Q$  to the Hamiltonian, where  $-\lambda$  is a ‘‘chemical potential’’ associated with the auxiliary particle number  $Q$ . The operator constraint  $Q = 1$  is imposed exactly on the expectation value of any operator  $O$  by differentiating with respect to the fugacity  $\zeta = e^{-\beta\lambda}$  and then taking the limit  $\lambda \rightarrow \infty$  [7]:

$$\langle O \rangle_C = \lim_{\lambda \rightarrow \infty} \frac{\frac{\partial}{\partial \zeta} \text{tr}[O e^{-\beta(H+\lambda Q)}]}{\frac{\partial}{\partial \zeta} \text{tr}[e^{-\beta(H+\lambda Q)}]}, \tag{C1}$$

where the trace is taken over the complete, enlarged Hilbert space. In particular, we state the following two results which are of use to us in this paper and which follow straightforwardly from the above (for details see [7]). First, the canonical partition function in the subspace  $Q = 1$  is

$$\begin{aligned} Z_C &= \lim_{\lambda \rightarrow \infty} \text{tr}[Qe^{-\beta(H+\lambda(Q-1))}] \\ &= \lim_{\lambda \rightarrow \infty} (e^{\beta\lambda} \langle Q \rangle_{GC}(\lambda)) Z_{Q=0}, \end{aligned} \quad (\text{C2})$$

where the subscripts  $GC$  and  $C$  denote the grand-canonical and the canonical ( $Q = 1$ ) expectation value, respectively. Second, the canonical  $Q = 1$  expectation value of any operator  $O$  having a zero expectation value in the  $Q = 0$  subspace is given by,

$$\langle O \rangle_C = \lim_{\lambda \rightarrow \infty} \frac{\langle O \rangle_{GC}(\lambda)}{\langle Q \rangle_{GC}(\lambda)} \quad (\text{C3})$$

Thus, we obtain the constrained  $d$ -electron Green function in terms of the grand-canonical one ( $G_d(\omega, T, \lambda)$ ) as

$$G_d(\omega) = \lim_{\lambda \rightarrow \infty} \frac{G_d(\omega, T, \lambda)}{\langle Q \rangle_{GC}(\lambda)} \quad (\text{C4})$$

In the enlarged Hilbert space ( $Q = 0, 1, 2, \dots$ )  $G_d(\omega, T, \lambda)$  may be expressed in terms of the pseudo-fermion and slave boson Green functions using Wick's theorem. It then follows from Eq. (C4) that the operator constraint  $Q = 1$  is imposed on the auxiliary Green's functions by simply taking the limit  $\lambda \rightarrow \infty$  of the respective unconstrained functions. Clearly, by this procedure all excitation energies of pseudo-fermions and slave bosons are shifted to  $\infty$ . It is therefore convenient to re-define the auxiliary particle frequency scale as  $\omega \rightarrow \omega + \lambda$  before taking the limit  $\lambda \rightarrow \infty$ . Note that this does not affect the energy scale of physical quantities (like the local  $d$  electron Green's function), which is the *difference* between the the pseudo-fermion and the slave-boson energy.



**APPENDIX D: NCA CALCULATION OF THE AUXILIARY SPECTRAL  
FUNCTIONS  $A_{F,B}^{\pm}$**

In order to enter the asymptotic power law regime of the auxiliary spectral functions and to compare with the  $T=0$  results of the NRG, the NCA must be evaluated for temperatures several orders of magnitude below  $T_0$ , the low temperature scale of the model. The equations are solved numerically by iteration. In this appendix the two main procedures are described to make the diagrammatic auxiliary particle technique suitable for the lowest temperatures.

The grand-canonical expectation value of the auxiliary particle number appearing in Eq. (C4) is given in terms of the (unprojected) auxiliary particle spectral functions  $A_{f,b}^+(\omega, T, \lambda)$  by,

$$\langle Q \rangle_{GC}(\lambda) = \int d\omega [f(\omega) \sum_{\sigma} A_{f\sigma}^+(\omega, T, \lambda) + b(\omega) A_b^+(\omega, T, \lambda)] \quad (\text{D1})$$

where  $f(\omega)$ ,  $b(\omega)$  denote the Fermi and Bose functions. Substituting this into the expression (C2) for the canonical partition function we obtain after carrying out the transformation  $\omega \rightarrow \omega + \lambda$ , and taking the limit  $\lambda \rightarrow \infty$

$$\begin{aligned} e^{-\beta F_{imp}(T)} &= \frac{Z_C}{Z_{Q=0}} = \lim_{\lambda \rightarrow \infty} e^{\beta \lambda} \langle Q \rangle_{GC}(\lambda) \\ &= \int d\omega e^{-\beta \omega} [\sum_{\sigma} A_{f\sigma}^+(\omega, T) + A_b^+(\omega, T)], \end{aligned} \quad (\text{D2})$$

where  $A_{f,b}^+(\omega, T)$  are now the projected spectral functions as defined in Eq. (5), and by definition  $F_{imp} = -\frac{1}{\beta} \ln(Z_C/Z_{Q=0})$  is the impurity contribution to the Free energy.

The numerical evaluation of expectation values like  $\langle Q \rangle_{GC}(\lambda \rightarrow \infty)$  (Eq. (D2)) or  $\Sigma_{c\sigma}(\omega, T, \lambda \rightarrow \infty)$  (Eq. (22)) is non-trivial (1) because at  $T = 0$  the auxiliary spectral functions  $A_{f,b}^+(\omega, T)$  are divergent at the threshold frequency  $E_0$ , where the exact position of  $E_0$  is a priori not known, and (2) because the Boltzmann factors  $e^{-\beta \omega}$  diverge strongly for  $\omega < 0$ . Therefore, we apply the following transformations:

(1) Before performing the projection  $\omega \rightarrow \omega + \lambda$ ,  $\lambda \rightarrow \infty$  we re-define the frequency scale of all auxiliary particle functions  $A_{f,b}^{\pm}$  according to  $\omega \rightarrow \omega + \lambda_0$ , where  $\lambda_0$  is a finite parameter. In each iteration  $\lambda_0$  is then determined such that

$$\int d\omega e^{-\beta\omega} [\sum_{\sigma} A_{f\sigma}^+(\omega) + A_b^+(\omega)] = 1 \quad (\text{D3})$$

where  $A_{f,b}^+(\omega) = \lim_{\lambda \rightarrow \infty} A_{f,b}^+(\omega + \lambda_0 + \lambda, T, \lambda)$  is now an auxiliary spectral function with the new reference energy. It is seen from Eq. (D2) that  $\lambda_0(T) = F_{imp}(T) = F_{Q=1}(T) - F_{Q=0}(T)$ , i.e.  $\lambda_0$  is the chemical potential for the auxiliary particle number  $Q$ , or equivalently the impurity contribution to the Free energy. The difference of the Free energies becomes equal to the threshold energy  $E_0 = E_{Q=1}^{GS} - E_{Q=0}^{GS}$  at  $T = 0$ , so the energy scale of the shifted spectral functions defined above coincides exactly with that of the NRG spectral functions defined in (5). More importantly, however, the above way of determining a ‘‘threshold’’ is less ad hoc than, for example, defining it by a maximum in some function appearing in the NCA equations. It is also seen from Eq. (D3) that this procedure defines the frequency scale of the auxiliary particles such that the  $T = 0$  threshold divergence of the spectral functions is at the *fixed* frequency  $\omega = 0$ . This substantially increases the precision as well as the speed of numerical evaluations. Eq. (C4) for the projected  $d$  electron Green’s function becomes

$$G_d(\omega) = \lim_{\lambda \rightarrow \infty} e^{\beta\lambda} G_d(\omega, T, \lambda). \quad (\text{D4})$$

(2) The divergence of the Boltzmann factors implies that the self-consistent solutions for  $A_{f,b}^+(\omega)$  vanish exponentially  $\sim e^{\beta\omega}$  for negative frequencies. It is convenient, not to formulate the self-consistent equations in terms of  $A_{f,b}^{\pm}$  like in earlier evaluations [8], but to define new functions  $\tilde{A}_{f,b}(\omega)$  and  $\text{Im}\tilde{\Sigma}_{f,b}(\omega)$  such that

$$A_{f,b}^+(\omega) = f(-\omega) \tilde{A}_{f,b}(\omega) \quad (\text{D5})$$

$$\text{Im}\Sigma_{f,b}(\omega) = f(-\omega) \text{Im}\tilde{\Sigma}_{f,b}(\omega). \quad (\text{D6})$$

After fixing the chemical potential  $\lambda_0$  and performing the projection onto the physical subspace, the canonical partition function (Eq. (C2)) behaves as  $\lim_{\lambda \rightarrow \infty} e^{\beta(\lambda - \lambda_0)} Z_C(T) = 1$ , and it follows immediately from the definition of  $A_{f,b}^-$  that

$$A_{f,b}^-(\omega) = f(\omega) \tilde{A}_{f,b}(\omega). \quad (\text{D7})$$

In this way all exponential divergencies are absorbed by one single function for each particle species. The NCA equations in terms of these functions are free of divergencies of the statistical factors and read

$$\text{Im}\tilde{\Sigma}_{f\sigma}(\omega - i0, T) = V^2 \sum_k \frac{(1 - f(\epsilon_k))(1 - f(\omega - \epsilon_k))}{1 - f(\omega)} \tilde{A}_b(\omega - \epsilon_k) \quad (\text{D8})$$

$$\text{Im}\tilde{\Sigma}_b(\omega - i0, T) = V^2 \sum_{k,\sigma} \frac{f(\epsilon_k)(1 - f(\omega + \epsilon_k))}{1 - f(\omega)} \tilde{A}_{f\sigma}(\omega + \epsilon_k), \quad (\text{D9})$$

$$\langle Q \rangle(\lambda_0, \lambda \rightarrow \infty) = \int d\omega f(\omega) [\sum_{\sigma} \tilde{A}_{f\sigma}(\omega) + \tilde{A}_b(\omega)] = 1 \quad (\text{D10})$$

$$\text{Im}G_{d\sigma}(\omega - i0, T) = \int d\epsilon [f(\epsilon + \omega)f(-\epsilon) + f(-\epsilon - \omega)f(\epsilon)] \tilde{A}_{f\sigma}(\epsilon + \omega) \tilde{A}_b(\epsilon), \quad (\text{D11})$$

where the real parts of the self-energies  $\Sigma_f$ ,  $\Sigma_b$ ,  $\Sigma_c$  are determined from a Kramers–Kronig relation, and the auxiliary spectral functions are the imaginary parts of the Green’s functions,  $A_{f\sigma}^+(\omega) = -\text{Im}[(\omega + \lambda_0 - i0 - \epsilon_d - \Sigma_{f\sigma}(\omega - i0))^{-1}]$ ,  $A_b^+(\omega) = -\text{Im}[(\omega + \lambda_0 - i0 - \Sigma_b(\omega - i0))^{-1}]$ .

The above method allows to solve the NCA equations effectively for temperatures down to typically  $T = 10^{-4}T_0$ . It may be shown that the same procedure can also be applied to self-consistently compute vertex corrections [23] beyond the NCA.

## REFERENCES

- [1] P. W. Anderson, *Science* **235**, 1196 (1987).
- [2] N. Nagaosa and P. A. Lee, *Phys. Rev. Lett.* **64**, 2450 (1990); C. M. Varma, P. B. Littlewood, S. Schmitt–Rink, E. Abrahams, and A. E. Ruckenstein, *Phys. Rev. Lett.* **63**, 1996 (1987); P. W. Anderson, *Phys. Rev. Lett.* **65**, 2306 (1990).
- [3] S. E. Barnes, *J. Phys.* **F6**, 1375 (1976); **F7**, 2637 (1977).
- [4] G. Baskaran and P. W. Anderson, *Phys. Rev.* **B37**, 580 (1988); L. Ioffe and A. Larkin, *Phys. Rev.* **B39** 8988 (1989); N. Nagaosa and P. A. Lee, *Phys. Rev.* **B45**, 966 (1992).
- [5] G. Baym and L.P. Kadanoff, *Phys. Rev.* **124**, 287 (1961); G. Baym, *Phys. Rev.* **127** 1391 (1962).
- [6] A. C. Hewson, *The Kondo Problem to Heavy Fermions*, C.U.P (1993) gives an extensive discussion of the magnetic impurity problem.
- [7] P. Coleman, *Phys. Rev.* **B29**, 3035 (1984).
- [8] N. E. Bickers, *Rev. Mod. Phys.* **59**, 845 (1987); N. E. Bickers, D. L. Cox & J. W. Wilkins, *Phys. Rev.* **B36**, 2036 (1987).
- [9] H. Keiter and J. C. Kimball, *J. Appl. Phys.* **42**, 1460 (1971); N. Grewe and H. Keiter, *Phys. Rev. B* **24**, 4420 (1981);
- [10] Y. Kuramoto, *Z. Phys.* **B53**, 37 (1983); H. Kojima, Y. Kuramoto and M. Tachiki, *Z. Phys.* **B54**, 293 (1984); Y. Kuramoto and H. Kojima, *Z. Phys.* **B57**, 95 (1984); Y. Kuramoto, *Z. Phys.* **B65**, 29 (1986).
- [11] E. Müller–Hartmann, *Z. Phys.* **B57**, 281 (1984).
- [12] T. A. Costi, P. Schmitteckert, J. Kroha and P. Wölfle *Phys. Rev. Lett.* **73**, 1275 (1994).
- [13] T. A. Costi, P. Schmitteckert, J. Kroha and P. Wölfle *Physica C* **235–240**, 2287 (1994).

- [14] K. G. Wilson, *Rev. Mod. Phys.* **47**, 773 (1975); H. B. Krishnamurthy, J. W. Wilkins & K. G. Wilson, *Phys. Rev.* **B21**, 1044 (1980).
- [15] T. A. Costi, A. C. Hewson and V. Zlatić *J. Phys.: Cond. Matt.* **6**, 2251 (1994); T. A. Costi, A. C. Hewson, *J. Phys.: Cond. Matt.* **5**, 361 (1993); T. A. Costi, A. C. Hewson, *Phil. Mag.* **B65**, 1165 (1992).
- [16] P. W. Anderson, *Phys. Rev. Lett* **18**, 1049 (1967).
- [17] K. D. Schotte and U. Schotte, *Phys. Rev.* **185**, 509 (1969).
- [18] N. Read, *J. Phys. C***18**, 2651 (1985).
- [19] B. Menge and E. Müller–Hartmann, *Z. Phys.* **B73**, 225 (1988).
- [20] J. Gruneberg and H. Keiter, *Physica B***171**, 39 (1991).
- [21] F. Anders and N. Grewe, *Europhys. Lett.* **26**, 551 (1994); F. Anders, *J. Phys. Cond. Mat.* **7**, 2801 (1995).
- [22] J. Kroha, P. J. Hirschfeld, K. A. Muttalib and P. Wölfle, *Solid State Commun.***83**, 1003 (1992).
- [23] J. Kroha, in preparation (1995).

## FIGURES

FIG. 1. (a) The lowest order contribution to the generating functional  $\Phi$ , and, (b), the renormalized vertex part  $\Lambda(i\omega_\nu, i\omega_\nu - i\omega)$ , entering the expression (26) for the d-electron Green's function (with frequency conservation we can omit  $i\omega_n$  in  $\Lambda$ ). The solid lines are for band electrons, the dashed lines are for pseudo-fermions and the wiggly lines are for slave-bosons.

FIG. 2. The  $T = 0$  NRG pseudo-fermion  $A_f^\pm$  (solid lines) and slave-boson  $A_b^\pm$  (dashed lines) spectral functions in the Kondo case  $\epsilon_d/\Delta = -4$ ,  $T_0/\Delta = 1.87 \times 10^{-2}$ ,  $n_d = 0.874$ . The + signs are for the spectral function above the threshold,  $E_0$ , and the circles are for the spectral function below the threshold. The arrow indicates the position of  $|\epsilon_d|$ .

FIG. 3. The  $T = 0$  NRG spectral functions  $A_{f,b}^\pm$  in the mixed valent regime  $\epsilon_d/\Delta = 0$ ,  $n_d = 0.314$  with notation as in Fig. 2.

FIG. 4. The  $T = 0$  NRG spectral functions  $A_{f,b}^\pm$  in the empty orbital regime  $\epsilon_d/\Delta = +2$ ,  $n_d = 0.172$ , with notation as in Fig. 2.

FIG. 5. The exponents  $\alpha_f$  ( $\diamond$ ),  $\alpha_b$  ( $\circ$ ) deduced from the asymptotic power law behaviour of the auxiliary spectral functions as calculated within the NRG for different values of the occupation  $n_d$ . The solid lines are the functions  $n_d - n_d^2/2$  and  $1 - n_d^2/2$ .

FIG. 6. The temperature dependence of the occupation number  $n_d(T)$  for different  $\epsilon_d$  (the curves are labeled by  $\epsilon_d/\Delta$ ). The high temperature limit of  $2/3$  (indicated by an arrow) is recovered in all cases.

FIG. 7. Comparison of the NRG ( $\diamond$ ) and NCA ( $\circ$ ) auxiliary spectral functions  $A_{f,b}^+$  (a-b),  $A_{f,b}^-$  (c-d) in the Kondo case  $\epsilon_d/\Delta = -4$ . The arrow indicates the position of  $|\epsilon_d|$ . The NRG results are for  $T = 0$  and the NCA results are for  $T = 1.0 \times 10^{-6}D$ . The divergence of the NCA spectral functions for  $\omega \rightarrow 0$  is cut off below the finite temperature  $T \ll T_0$ .

FIG. 8. Comparison of the NRG ( $\diamond$ ) and NCA ( $\circ$ ) auxiliary spectral functions  $A_{f,b}^+$  (a-b),  $A_{f,b}^-$  (c-d) in the mixed valent case  $\epsilon_d/\Delta = 0$ . The NRG results are for  $T = 0$  and the NCA results are for  $T = 1.0 \times 10^{-6}D$ .

FIG. 9. Comparison of the NRG ( $\diamond$ ) and NCA ( $\circ$ ) auxiliary spectral functions  $A_{f,b}^+$  (a-b),  $A_{f,b}^-$  (c-d) in the empty orbital case  $\epsilon_d/\Delta = +2$ . The NRG results are for  $T = 0$  and the NCA results are for  $T = 1.0 \times 10^{-6}D$ .

FIG. 10. The impurity spectral function in the Kondo regime  $\epsilon_d = -4\Delta$ ,  $T_0/\Delta = 1.87 \times 10^{-2}$ , for (a) high energies and, the low energy region (b)  $-5 \leq \omega/T_0 \leq 10$ , and (c)  $-2 \leq \omega/T_0 \leq +2$ . The dashed curve is the NRG result  $\rho_d^{NRG}$ , the dot-dashed curve is the NRG result without the vertex part in (33), and the solid curve is the NCA result. The NRG results are for  $T = 0$  and the NCA results are for  $T = 1.0 \times 10^{-6}D$ .

FIG. 11. The impurity spectral function in the mixed valent regime  $\epsilon_d/\Delta = 0$ , with notation as in Fig. 10. The NRG results are for  $T = 0$  and the NCA results are for  $T = 1.0 \times 10^{-6}D$ .

FIG. 12. The impurity spectral function in the empty orbital regime  $\epsilon_d/\Delta = +2$ , with notation as in Fig. 10. The NRG results are for  $T = 0$  and the NCA results are for  $T = 1.0 \times 10^{-6}D$ .

## TABLES

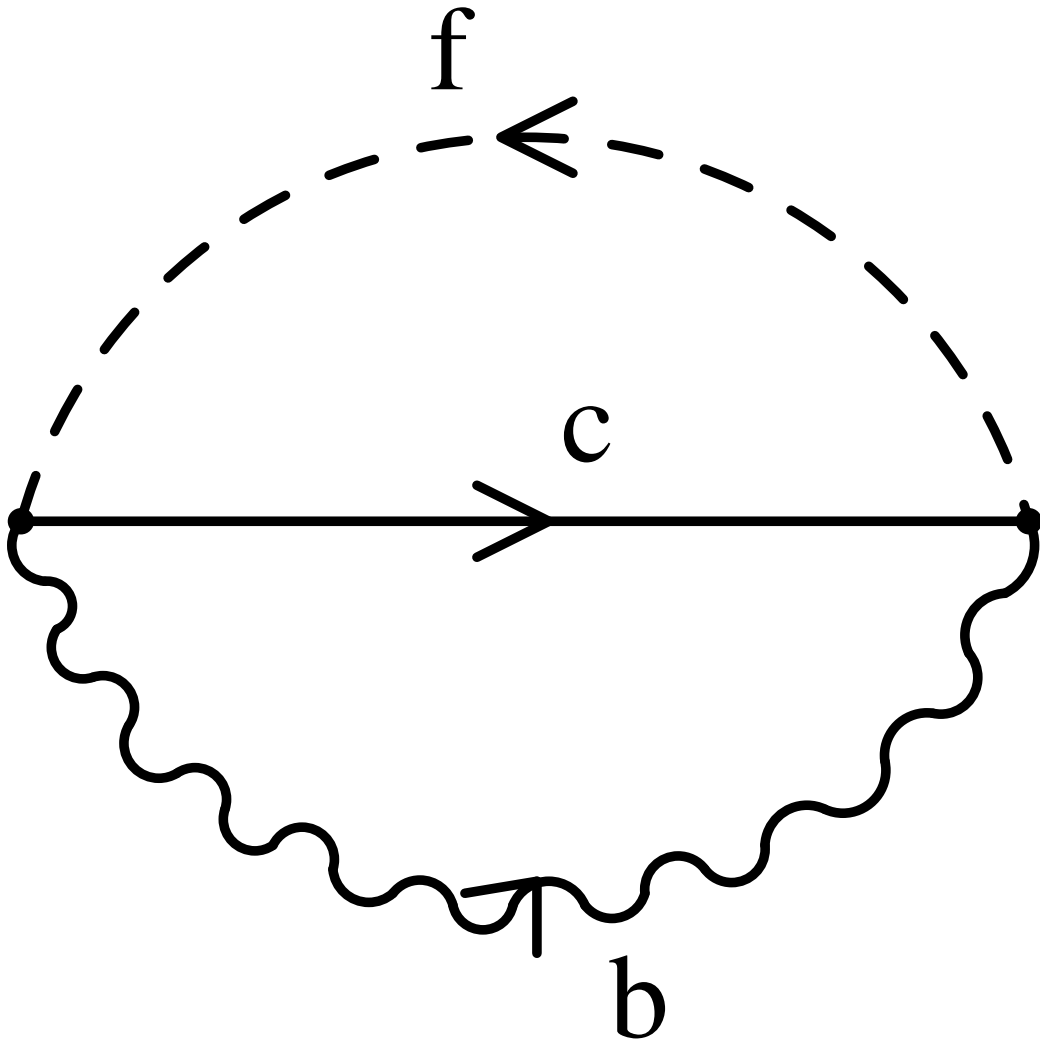
TABLE I. The threshold exponents  $\alpha_{f,b}$  for the auxiliary spectral functions  $A_{f,b}^{\pm} \sim |\omega - E_0|^{-\alpha_{f,b}}$ . The quantities  $\alpha'_{f,b}$  are  $n_d - n_d^2/2$  and  $1 - n_d^2/2$ , respectively where  $n_d = n_d^{NRG}$  is the impurity occupation calculated from the NRG partition function (quantities shown to 3 significant figures). The NCA results for the impurity occupation,  $n_d^{NCA}$ , are also shown. The impurity spectral density at the Fermi level calculated within the NCA,  $\rho_d^{NCA}(\epsilon_F)$ , and NRG,  $\rho_d^{NRG}(\epsilon_F)$ , are tabulated together with the % relative error in the Friedel sum rule,  $\rho_d(\epsilon_F) = \sin^2(\pi n_d/2)/\pi\Delta$ . The exponent  $\alpha_f$  is difficult to estimate close to  $n_d = 1$  due to the small Kondo scale and the slow asymptotic behaviour of the pseudo-fermion spectral function. The low energy scale  $T_0$  is  $T_K$  given by (27) in the Kondo regime,  $\Delta$  in the mixed valent regime and  $\epsilon_d$  in the empty orbital regime.

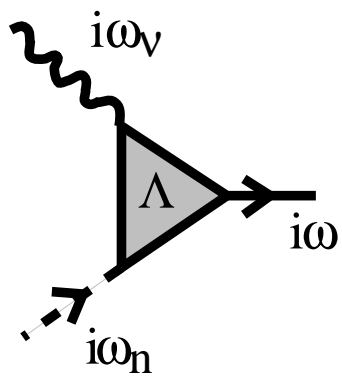
$\epsilon_d/\Delta$	$n_d^{NRG}$	$n_d^{NCA}$	$\rho_d^{NRG}(\epsilon_F)$	$\rho_d^{NCA}(\epsilon_F)$	$T_0/\Delta$	$\alpha_f$	$\alpha'_f$	$\alpha_b$	$\alpha'_b$
-7	0.947	—	—	—	$1.68 \times 10^{-4}$	0.501	0.499	0.552	0.552
-6	0.934	—	30.7 - 2.5%	—	$8.07 \times 10^{-4}$	0.499	0.498	0.563	0.564
-5	0.913	0.909	29.7 - 5.0%	31.1 - 0.3%	$3.88 \times 10^{-3}$	0.499	0.496	0.583	0.583
-4	0.874	0.865	30.1 - 1.7%	34.3 + 12.1%	$1.87 \times 10^{-2}$	0.493	0.492	0.618	0.619
-3	0.796	0.781	27.8 - 3.3%	30.4 + 7.8%	$8.98 \times 10^{-2}$	0.480	0.479	0.684	0.683
-2	0.648	0.641	23.4 + 1.4%	32.4 + 42.3%	$4.32 \times 10^{-1}$	0.439	0.438	0.790	0.790
-1	0.460	0.464	13.5 - 3%	28.5 + 102%	1	0.354	0.354	0.894	0.894
0	0.314	0.322	7.06 - 1%	26.3 + 252%	1	0.265	0.265	0.951	0.951
+1	0.226	0.232	3.80 - 1%	25.7 + 535%	1	0.200	0.200	0.975	0.974
+2	0.172	0.176	2.27 - 0.1%	17.5 + 637%	2	0.158	0.157	0.985	0.985



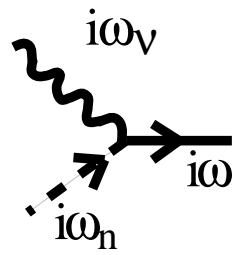
TABLE II. Coefficients  $C_{ii'}^\pm$

$ii'$	$C_{ii'}^+$	$C_{ii'}^-$
11	1	1
22	$\sqrt{\frac{2S(2S+2)}{(2S+1)(2S+1)}}$	1
33	1	$\sqrt{\frac{2S(2S+2)}{(2S+1)(2S+1)}}$
44	1	1
23	0	$\frac{1}{2S+1}$
32	$-\frac{1}{2S+1}$	0

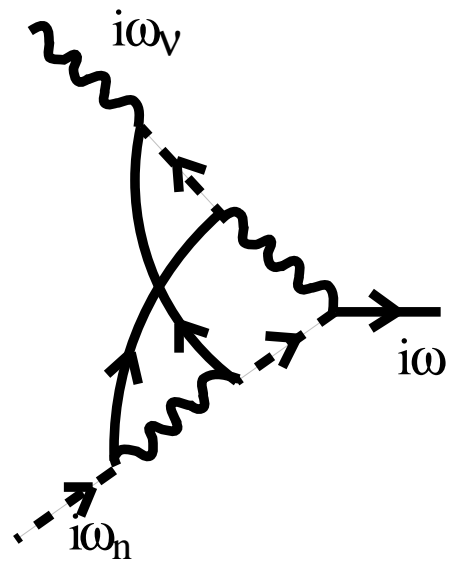




=



+



+ . . .

Fig2

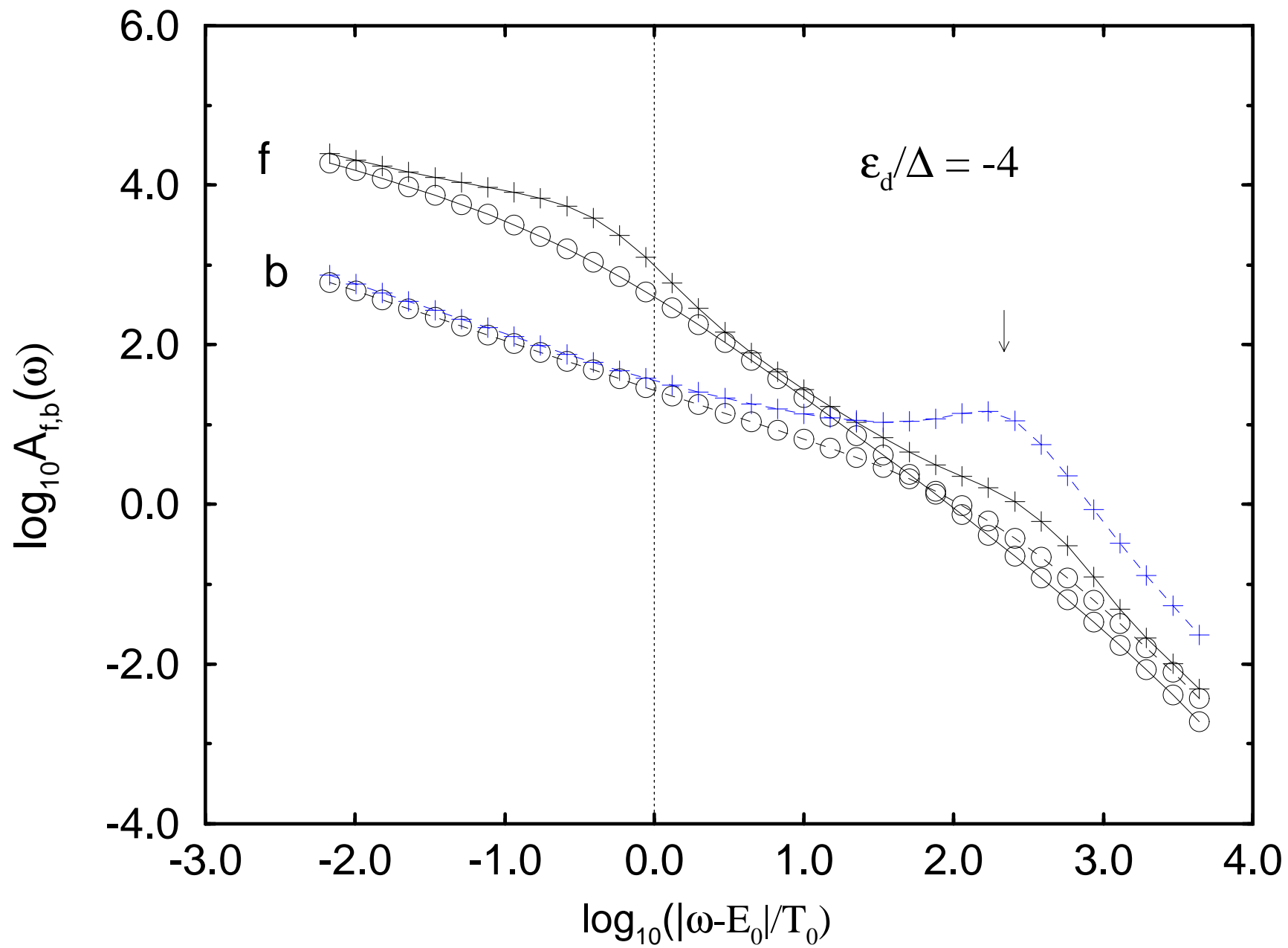


Fig3

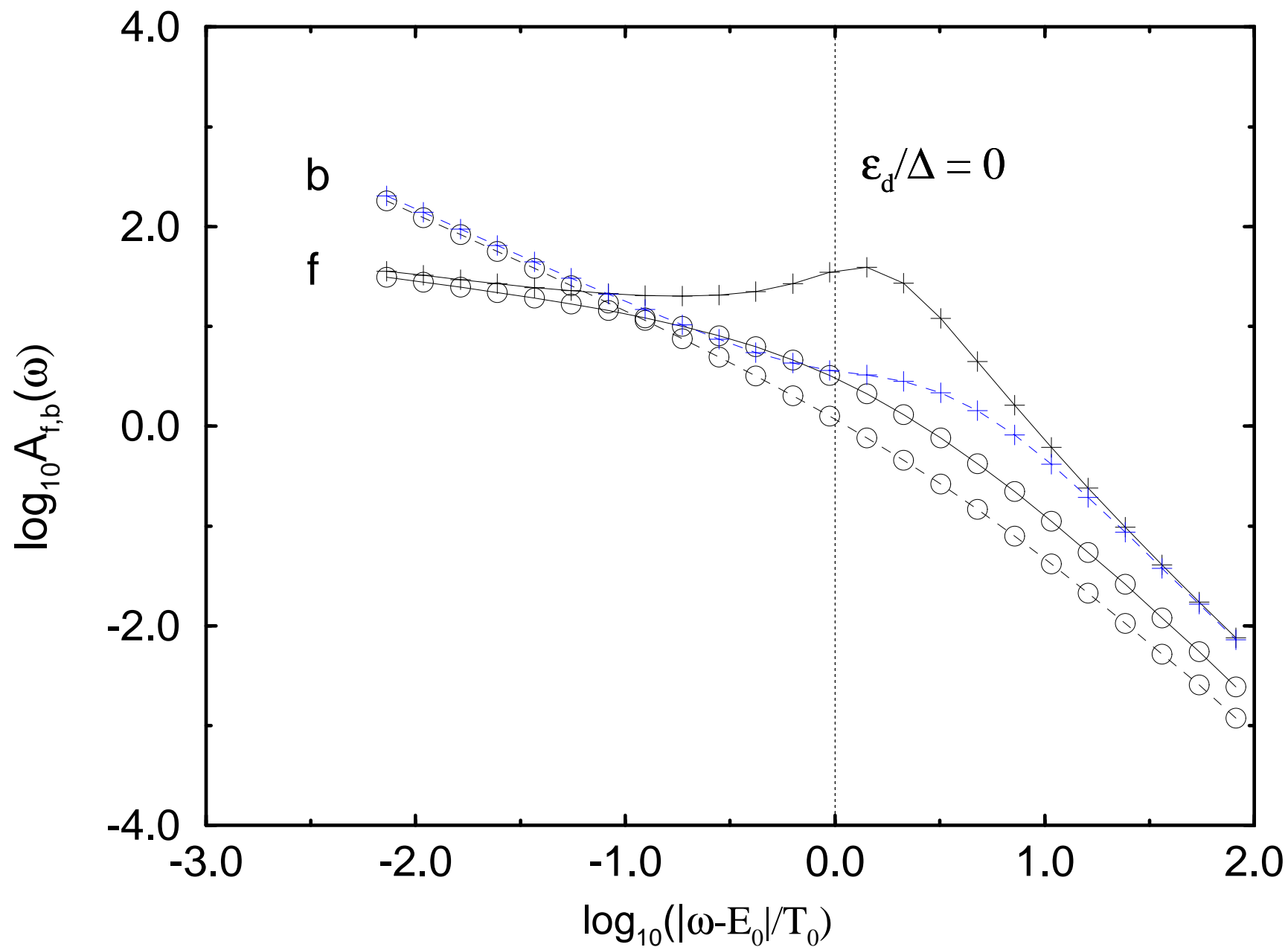
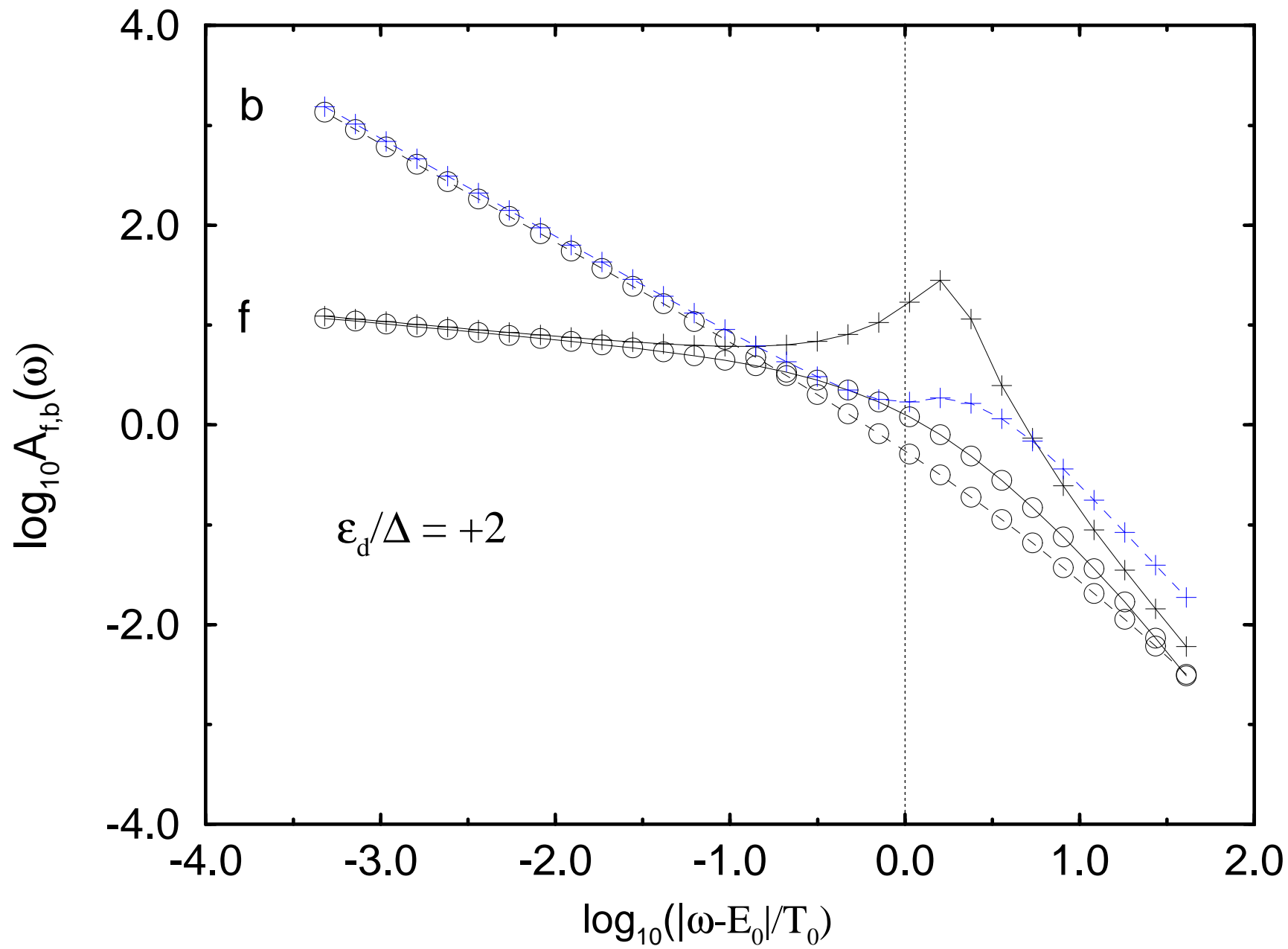


Fig4



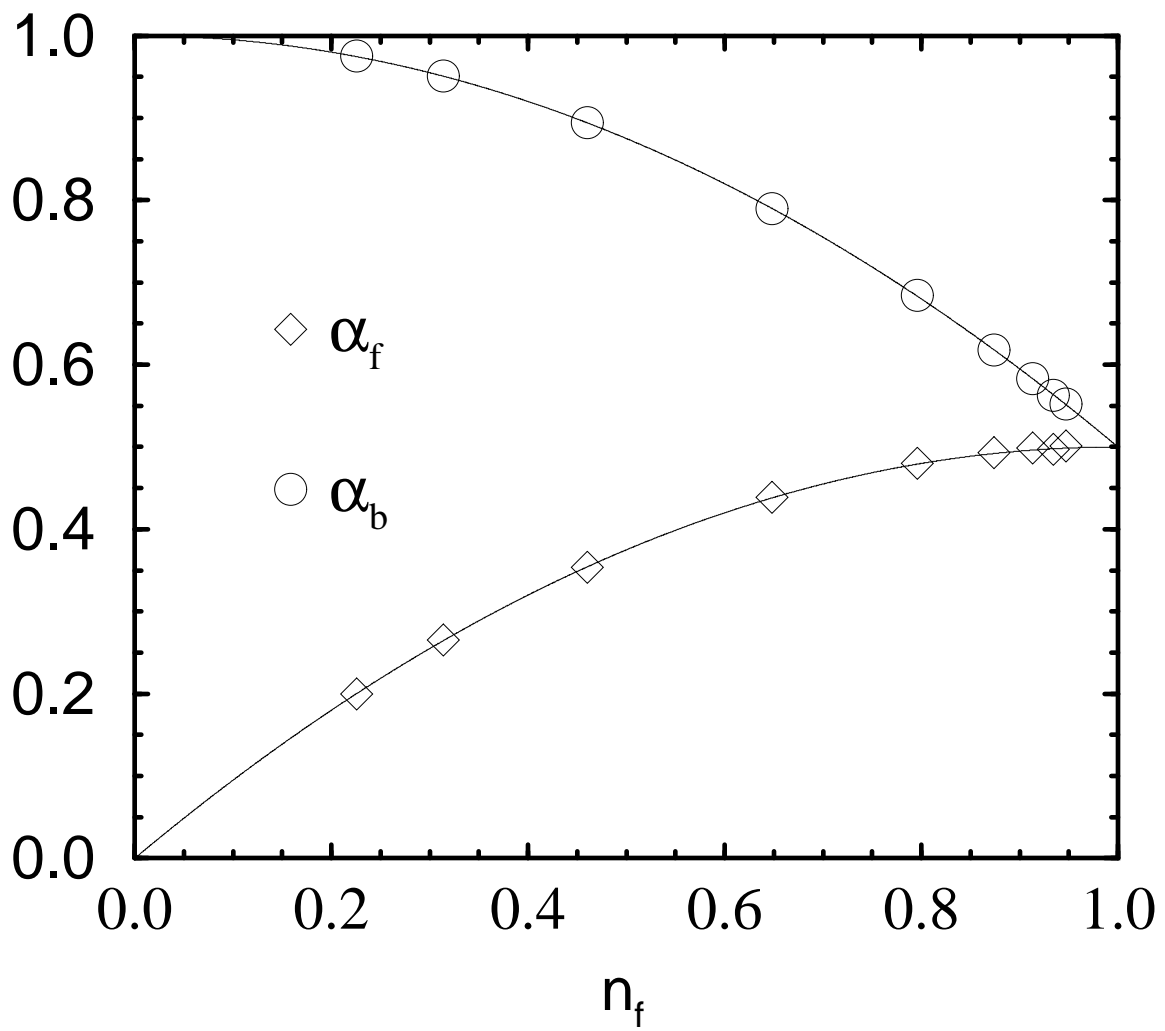






Fig7a

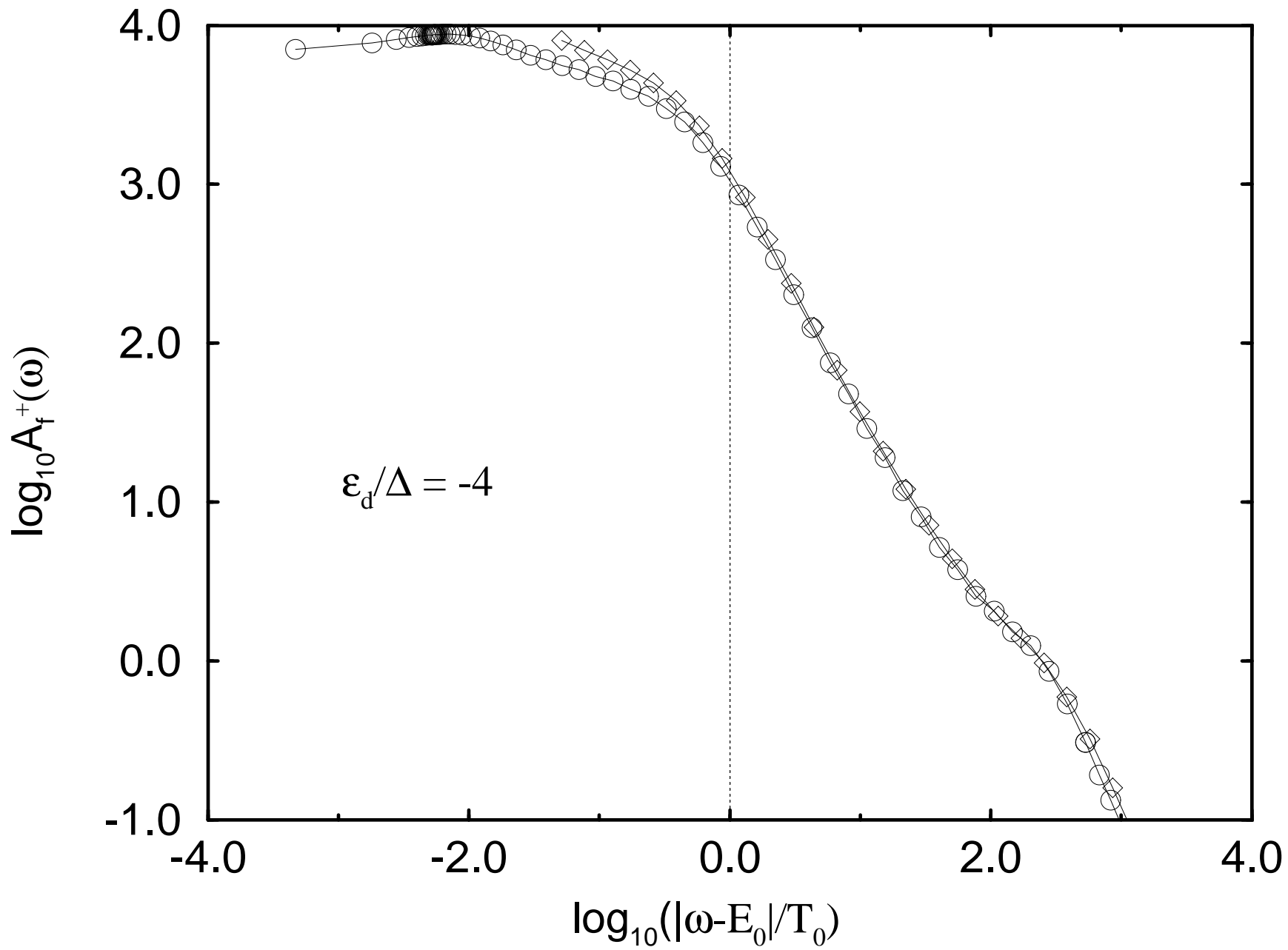


Fig. 7b

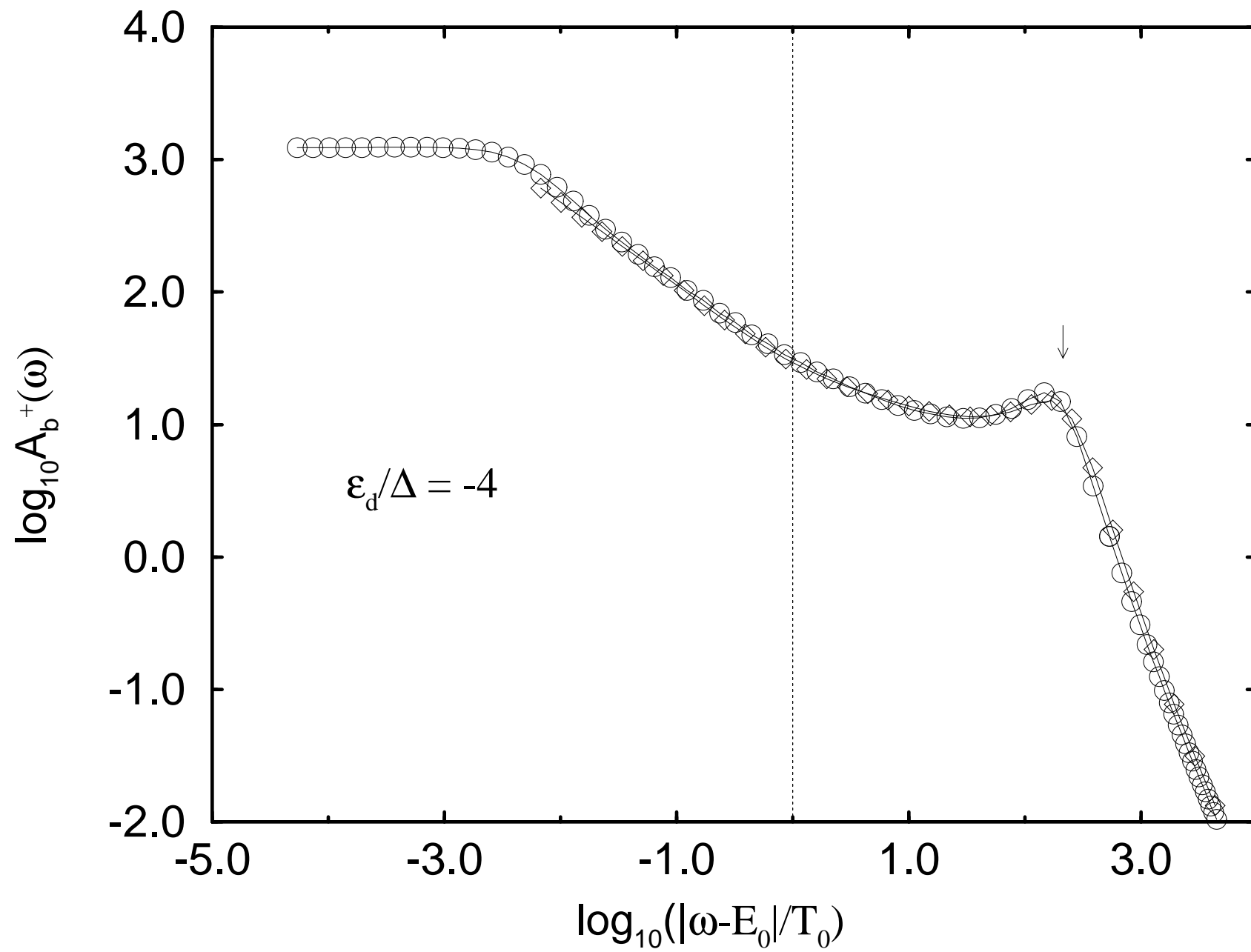


Fig7c

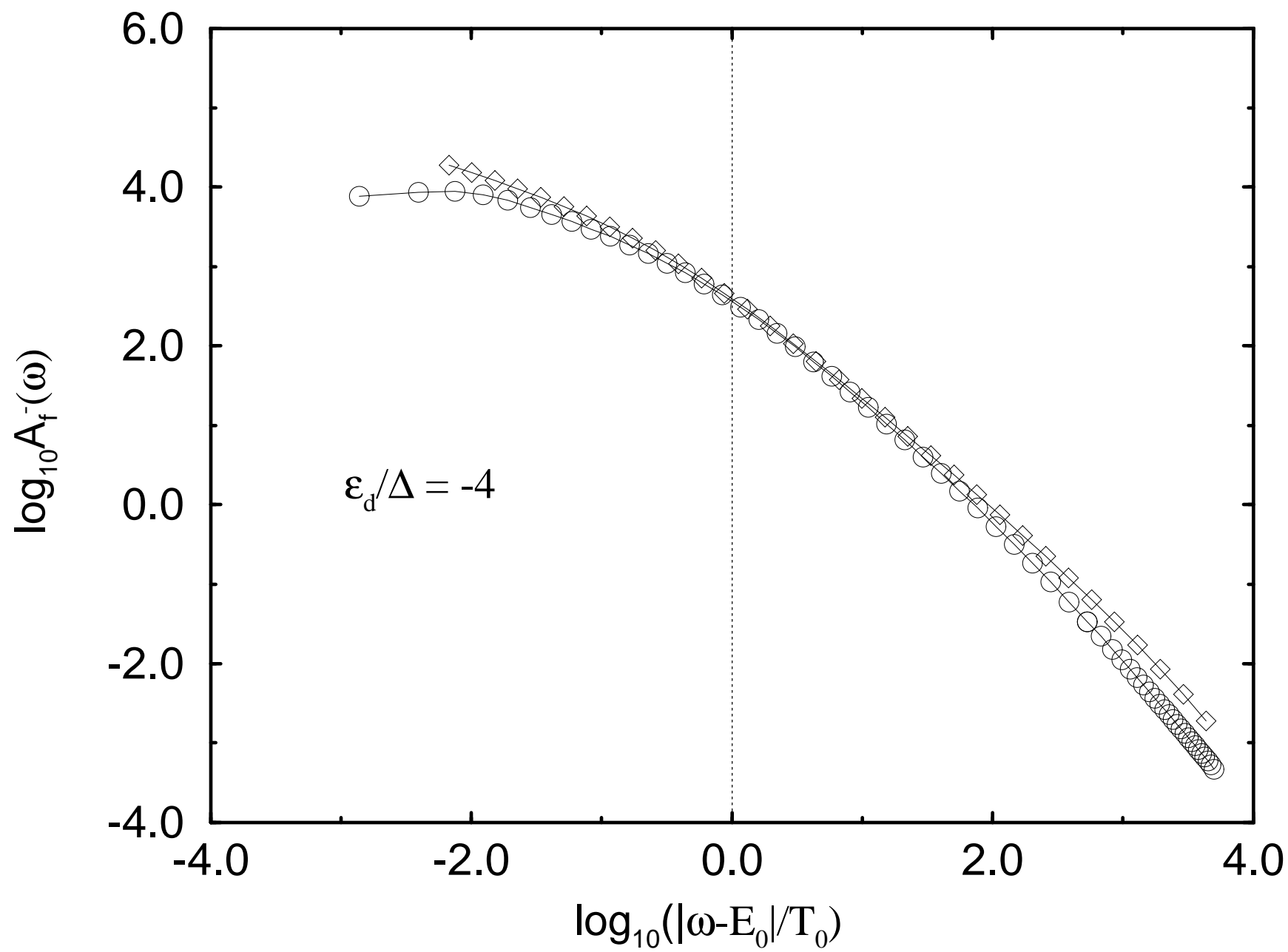


Fig7d

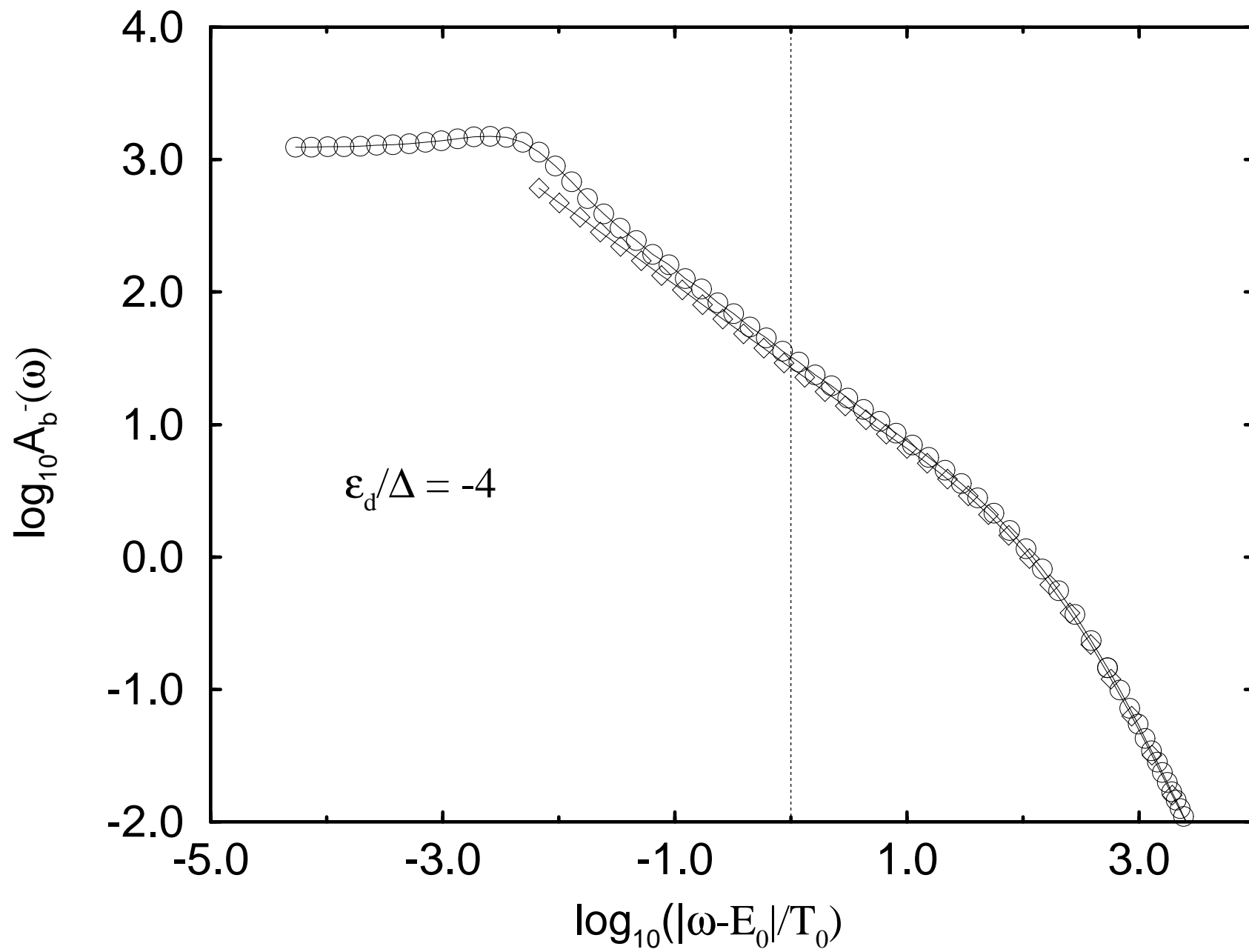


Fig8a

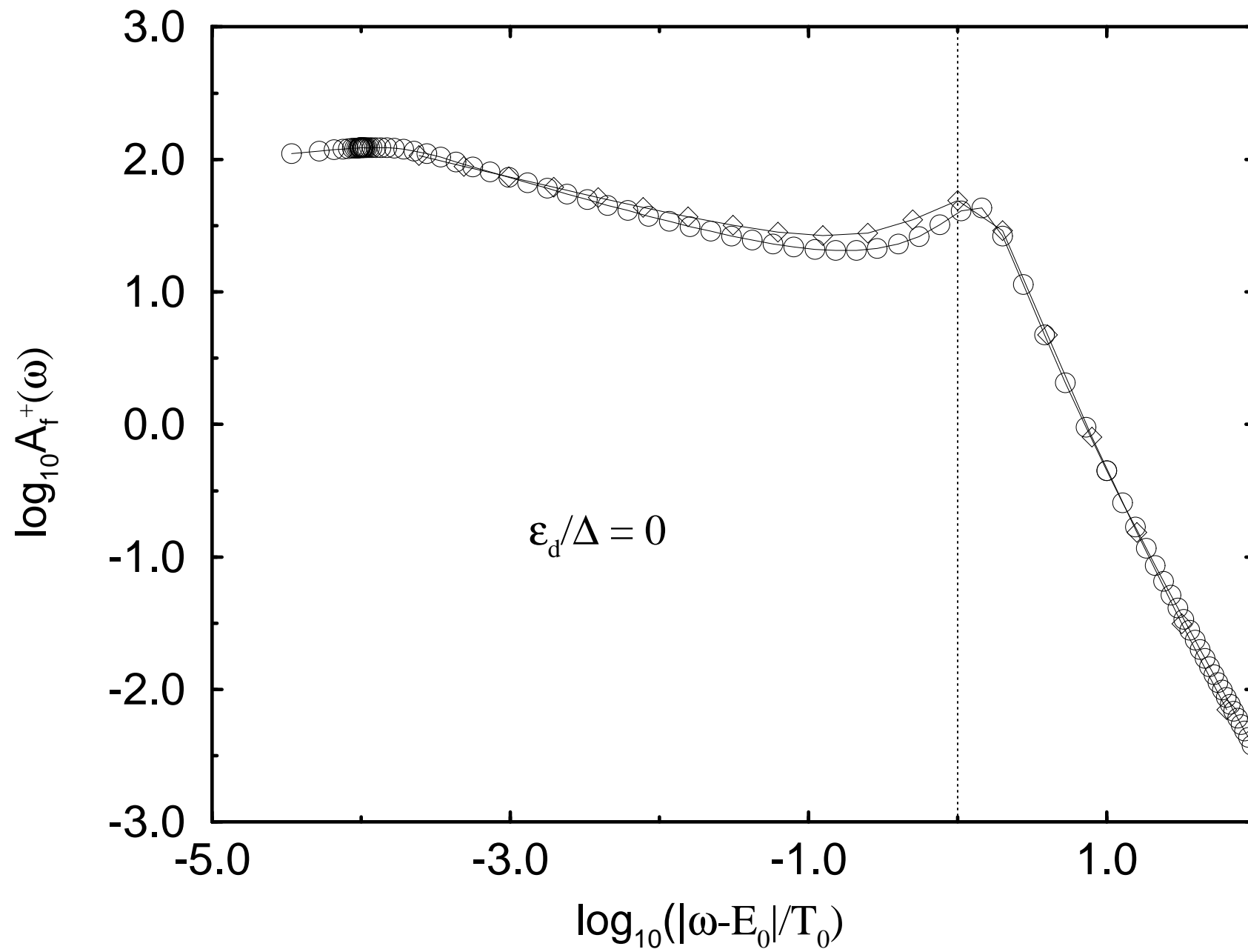


Fig8b

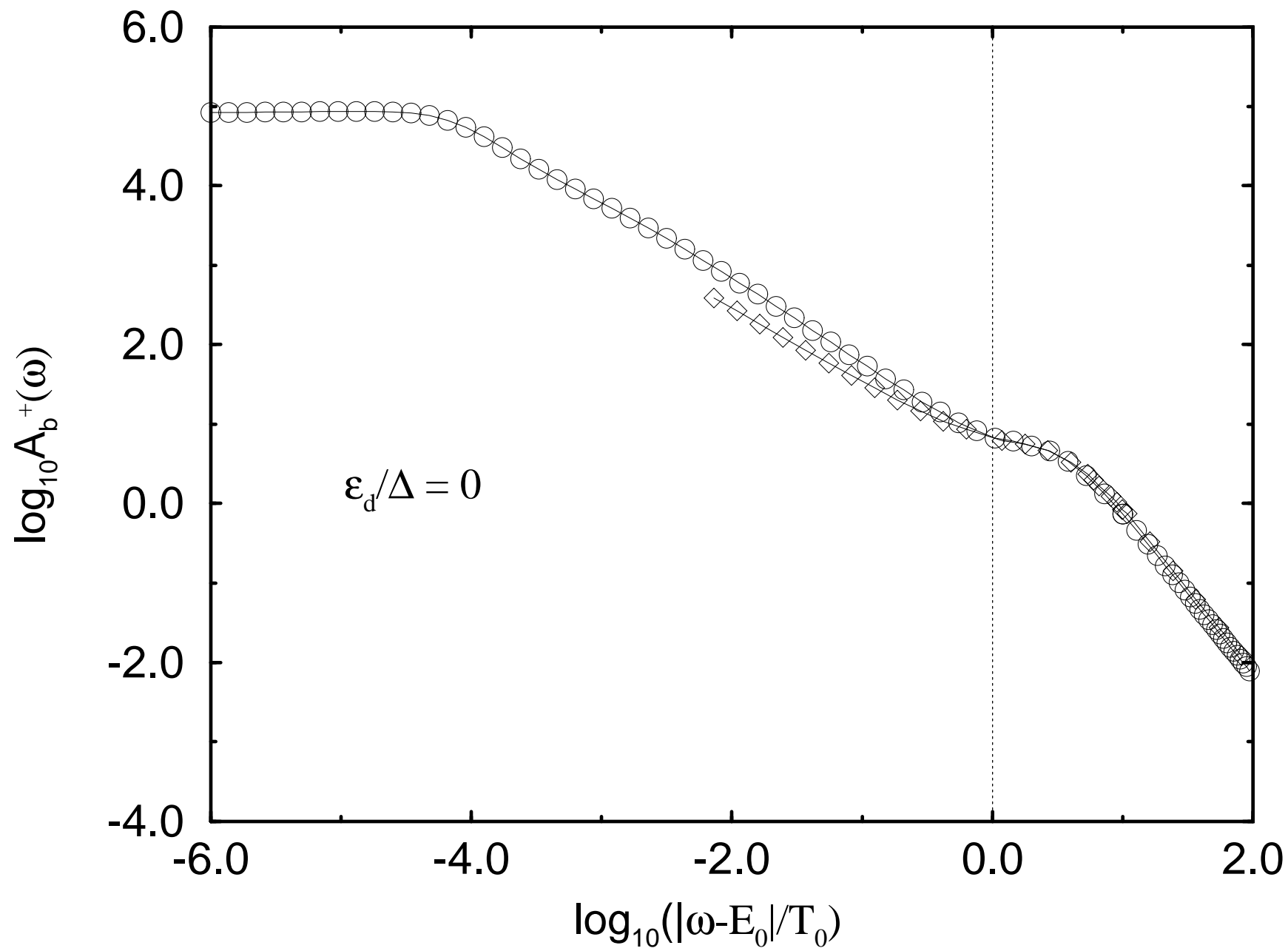


Fig8c

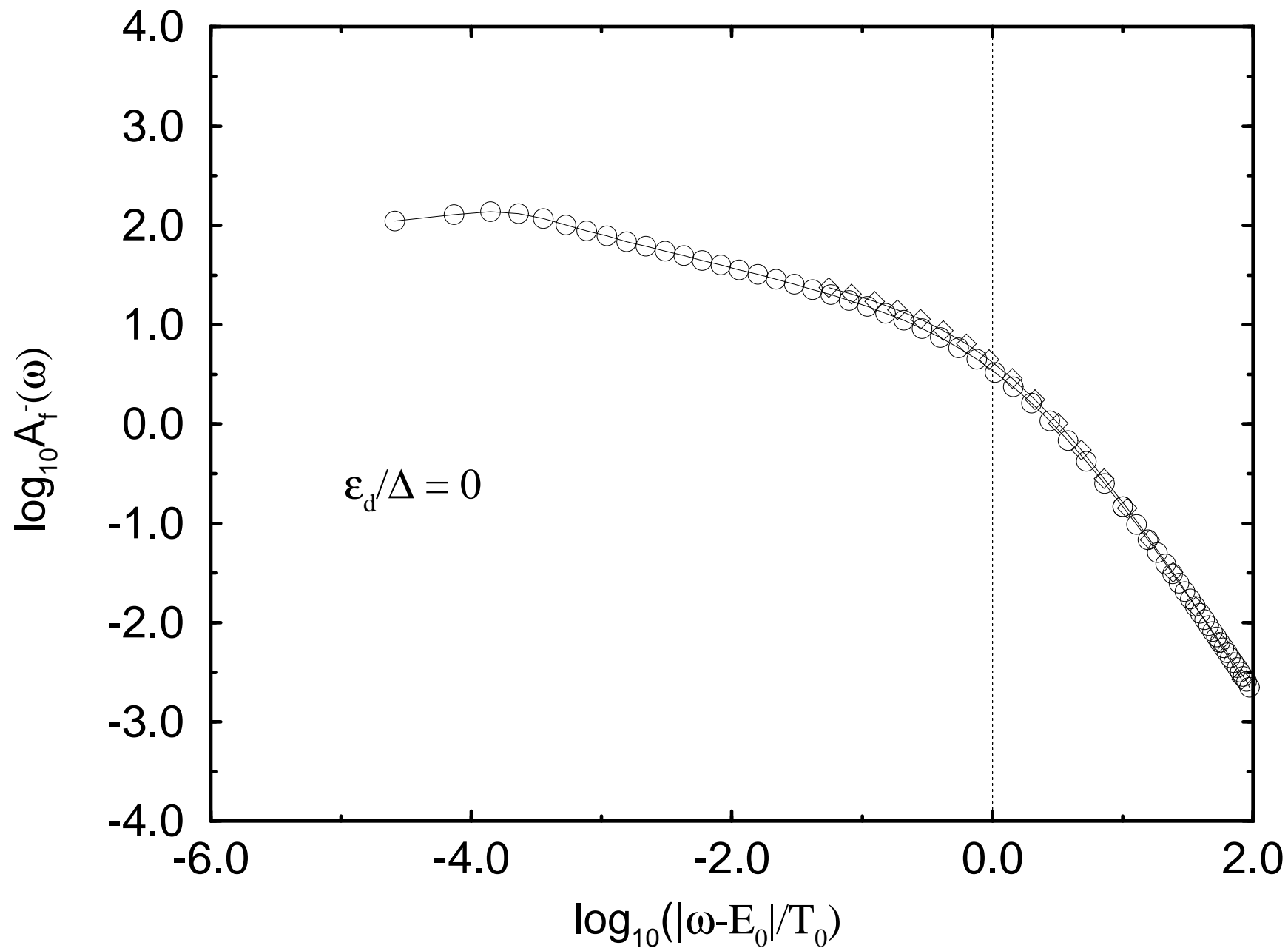


Fig8d

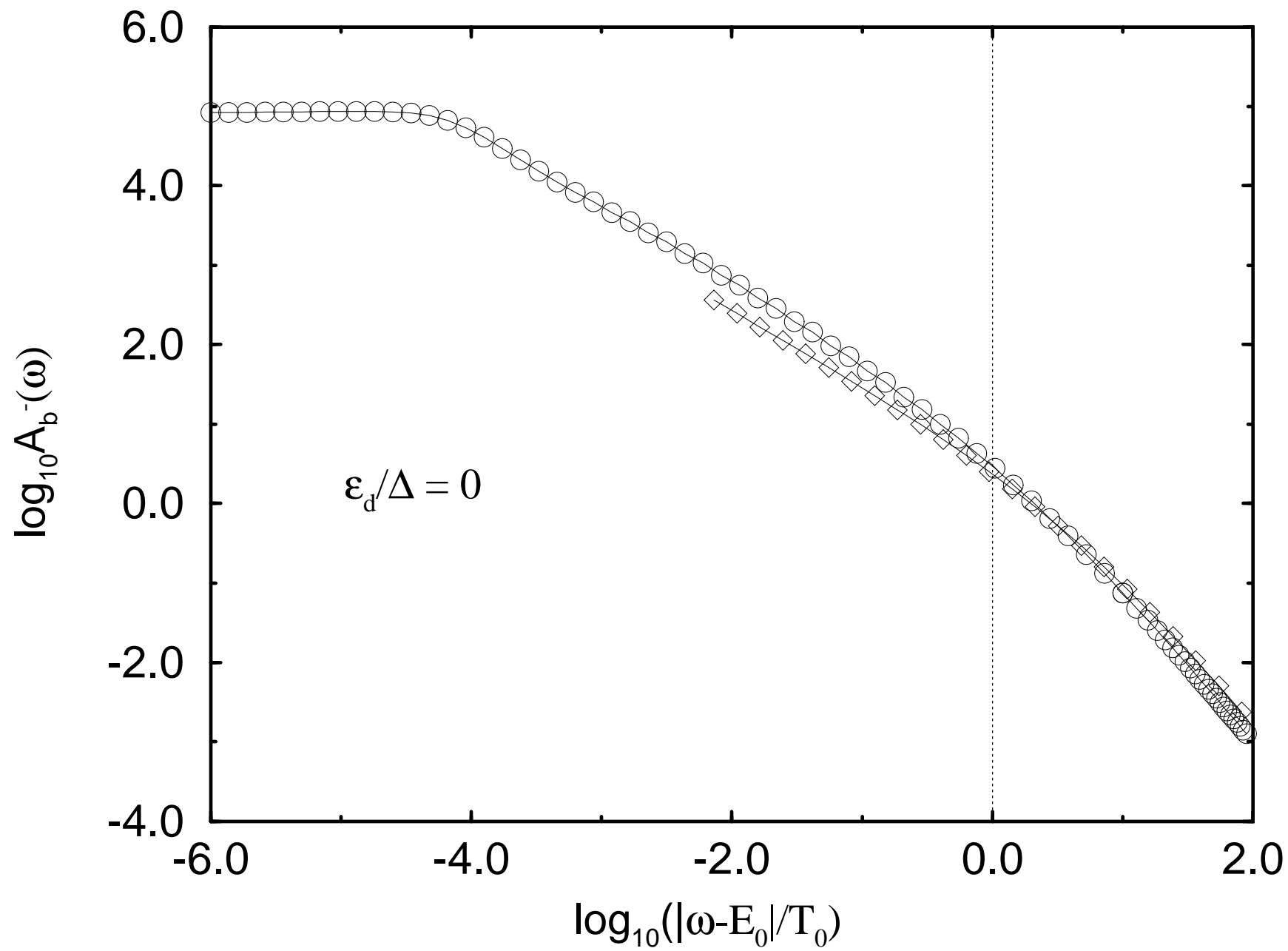




Fig9a

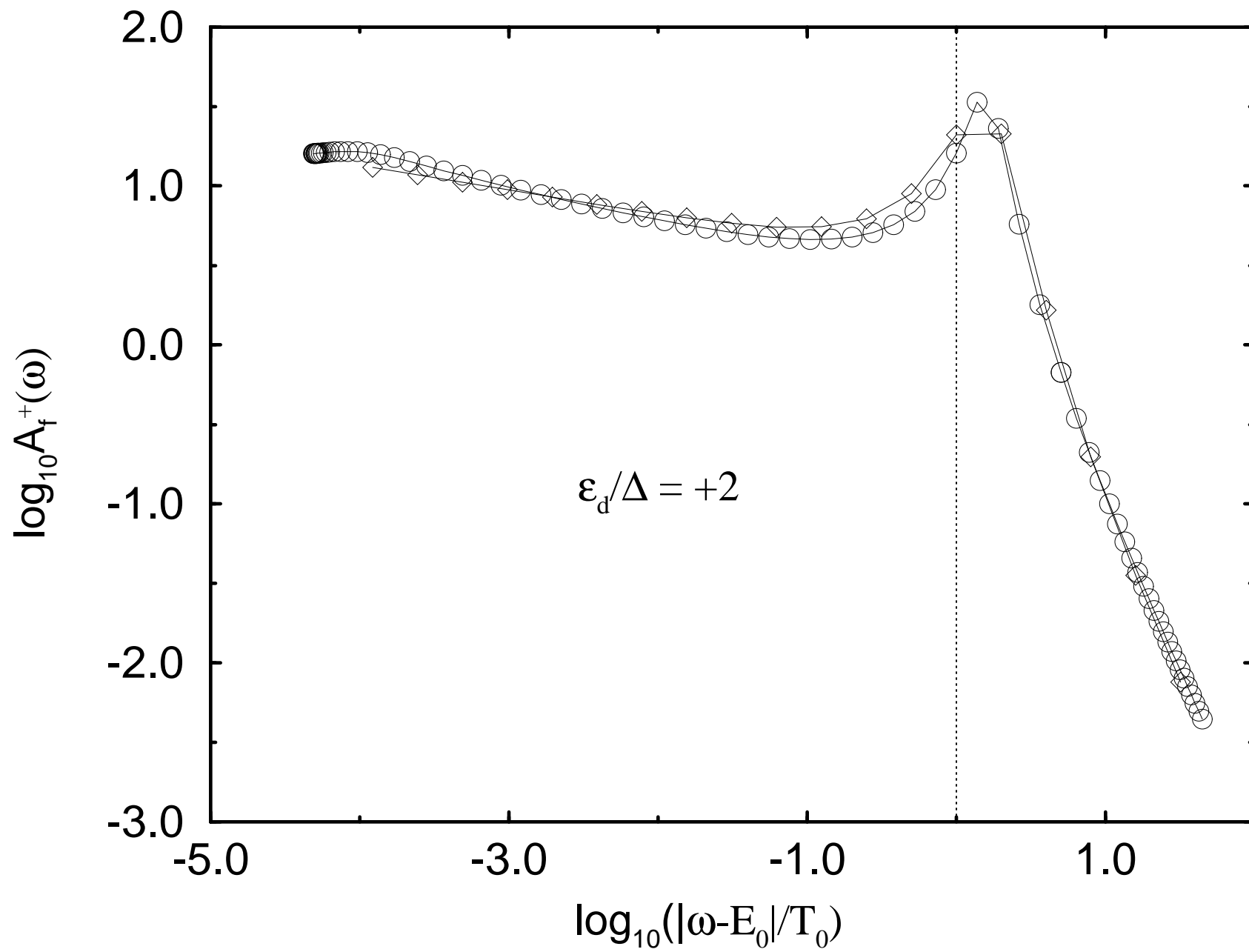


Fig9b

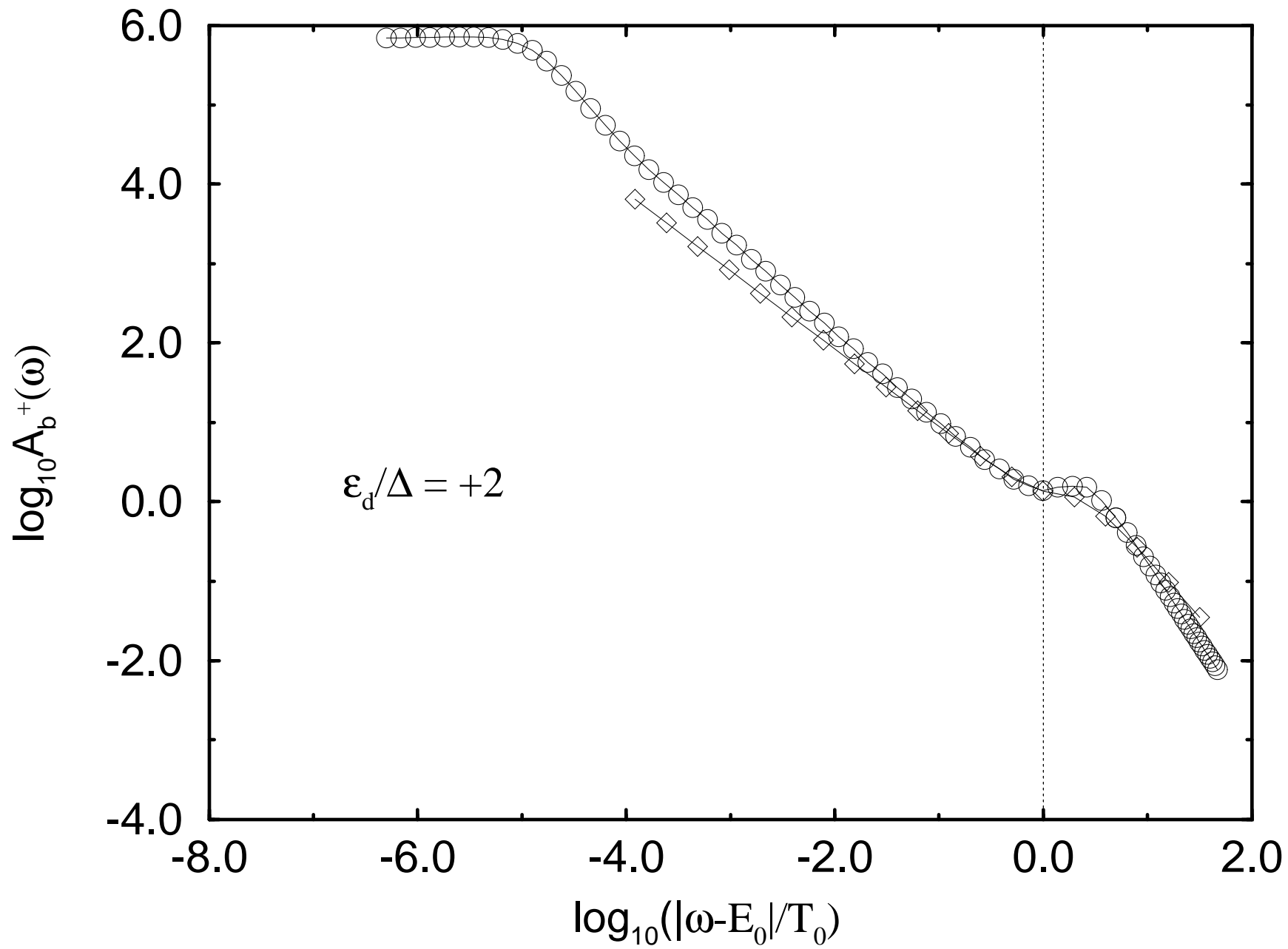


Fig9c

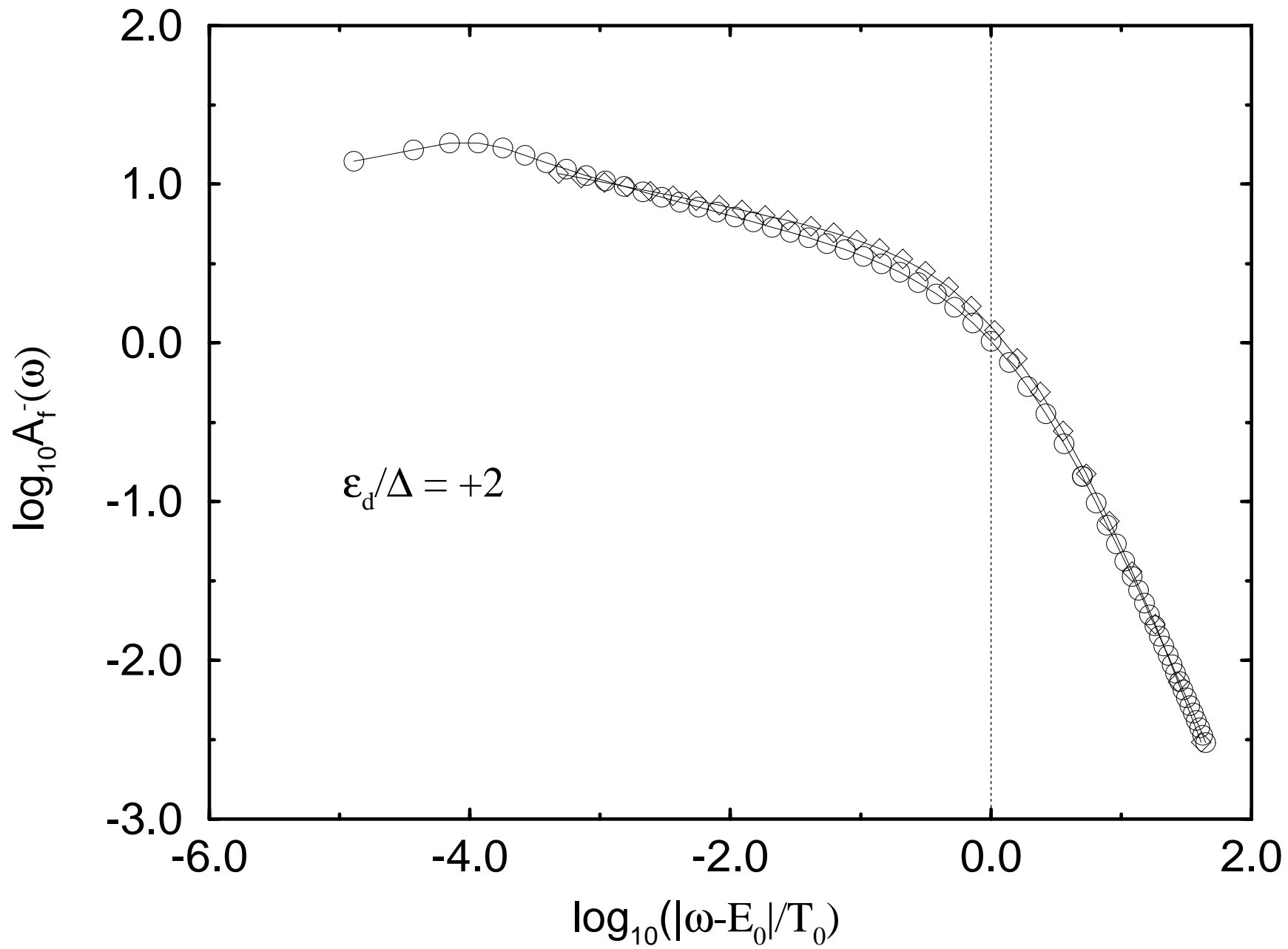


Fig9d

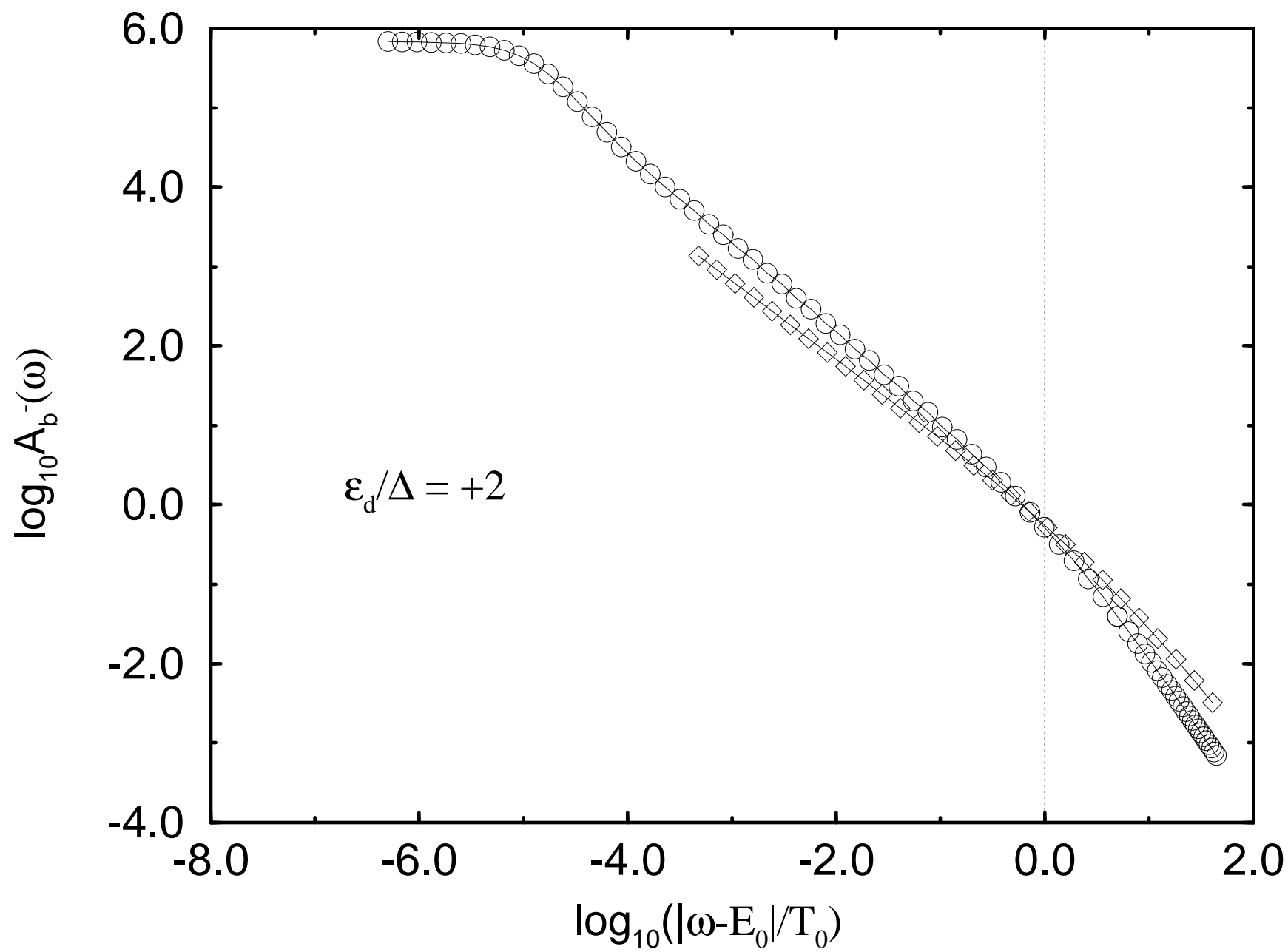


Fig10a

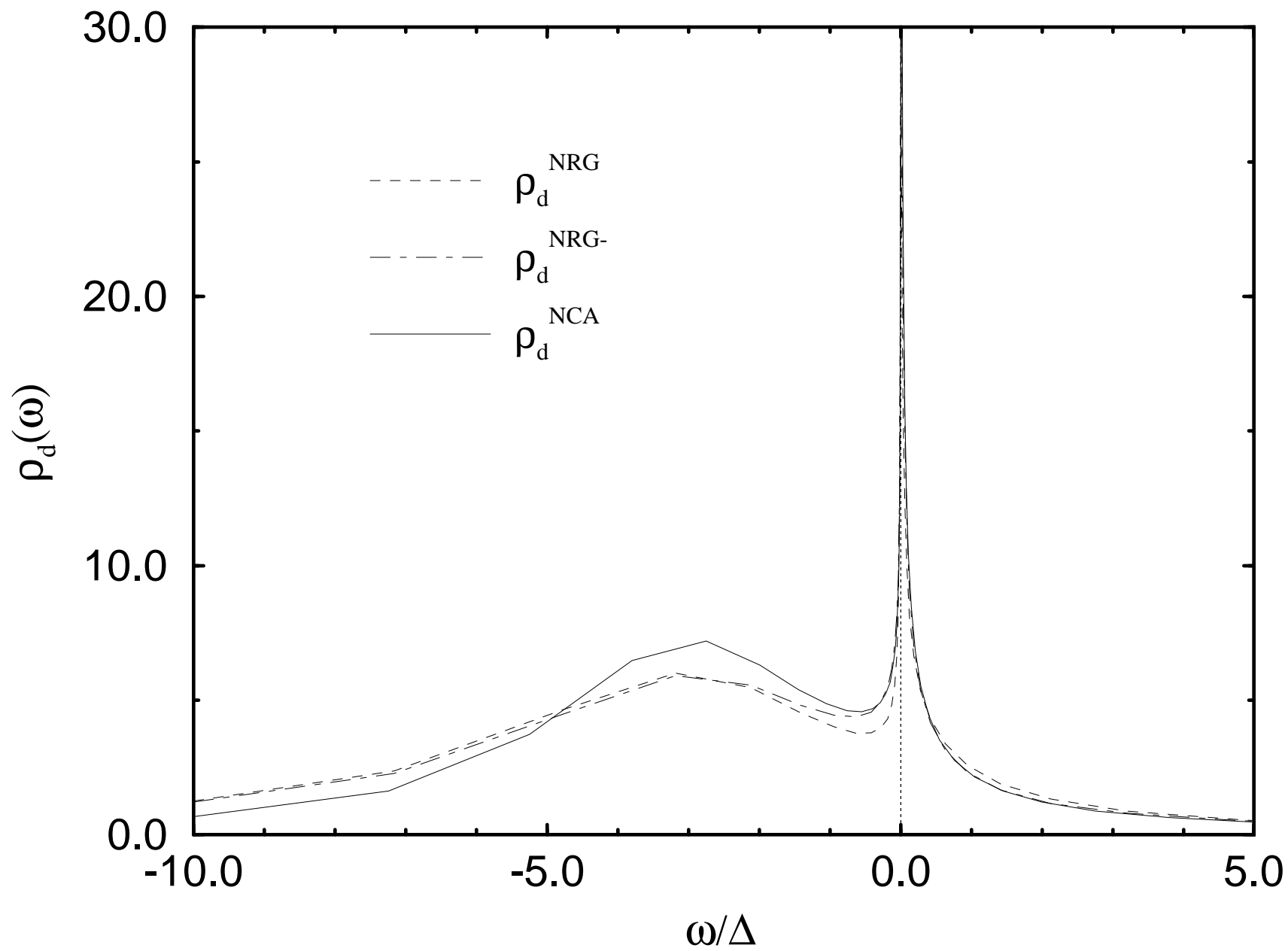


Fig10b

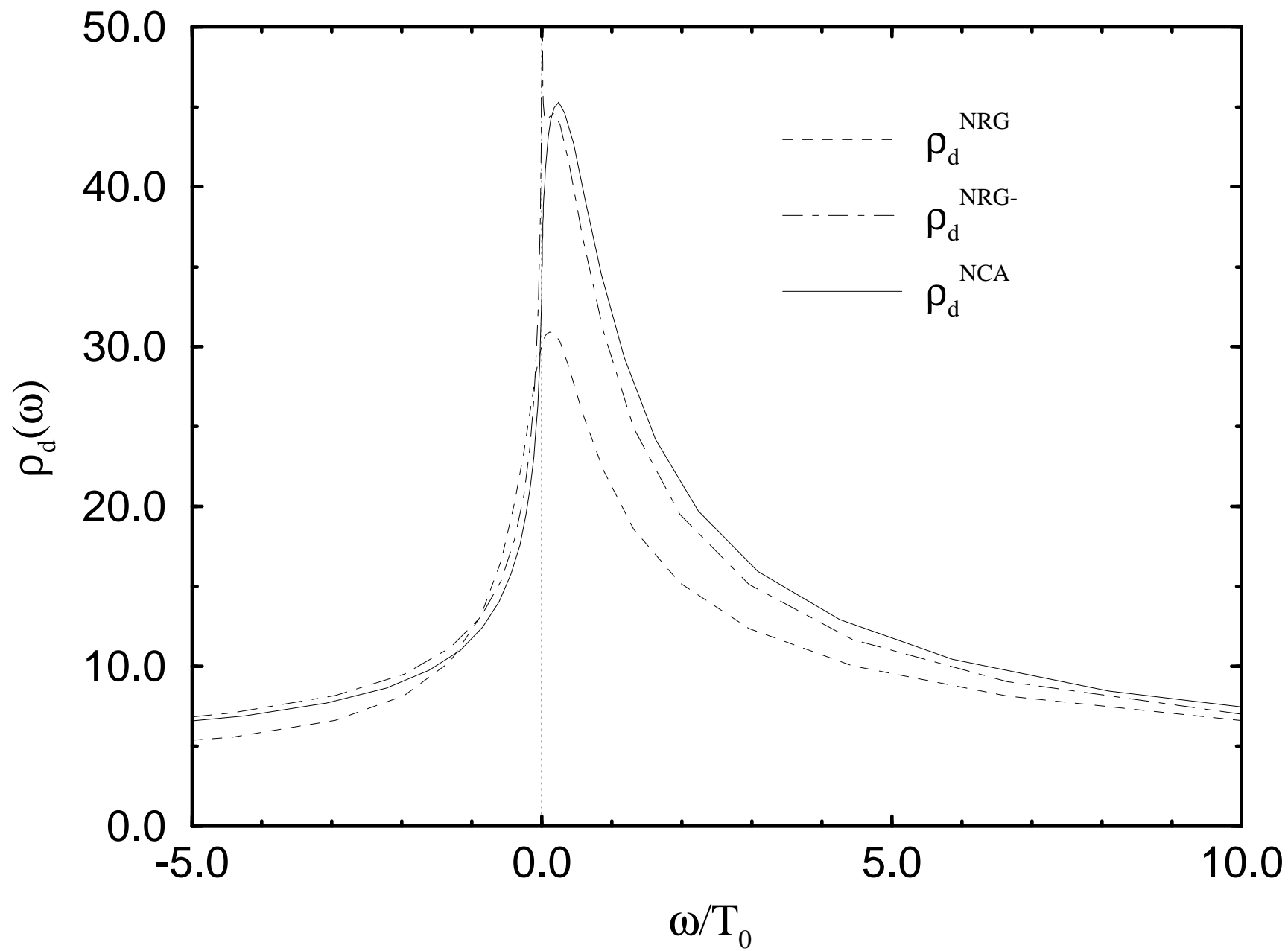


Fig10c

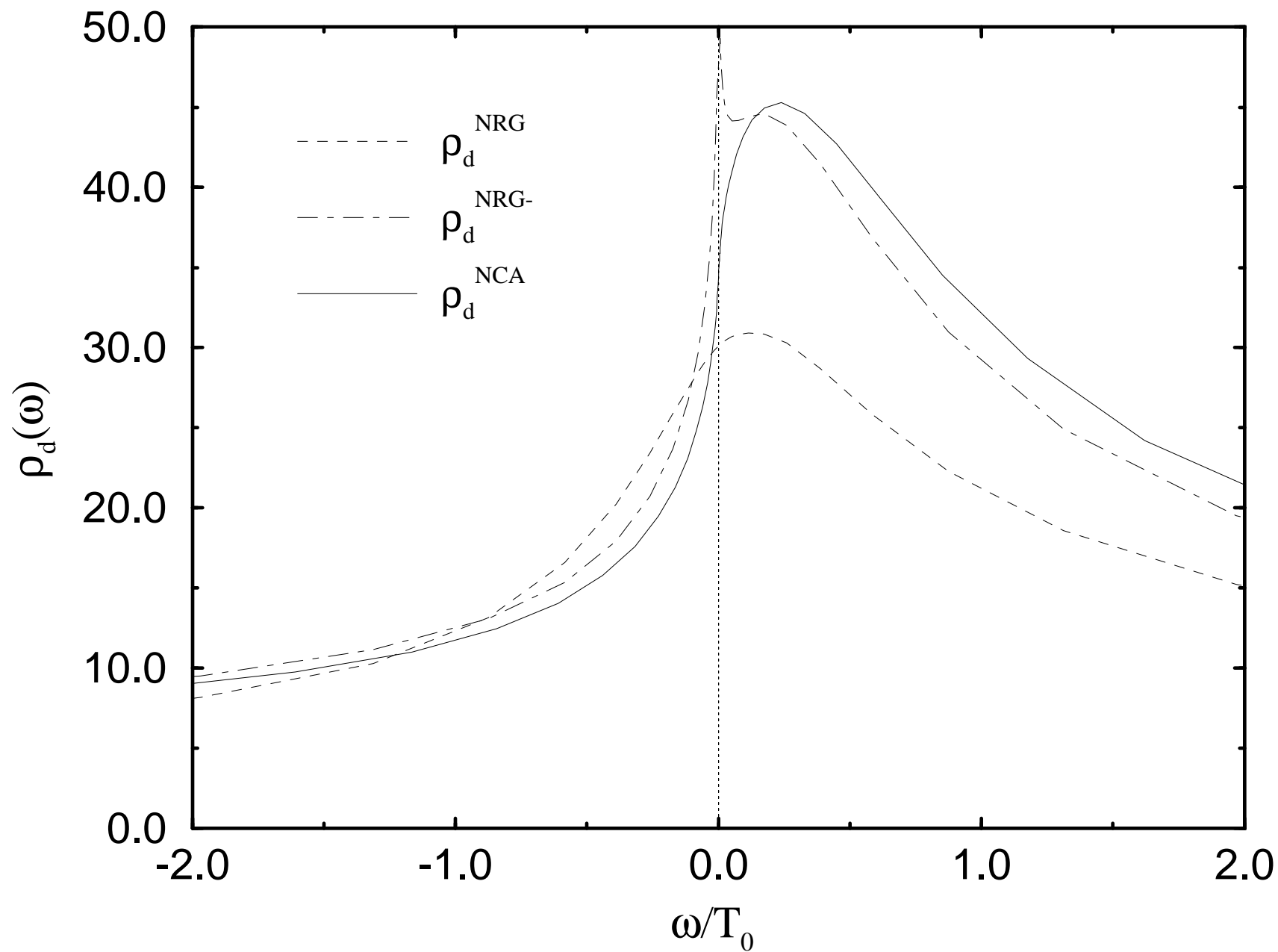


Fig11

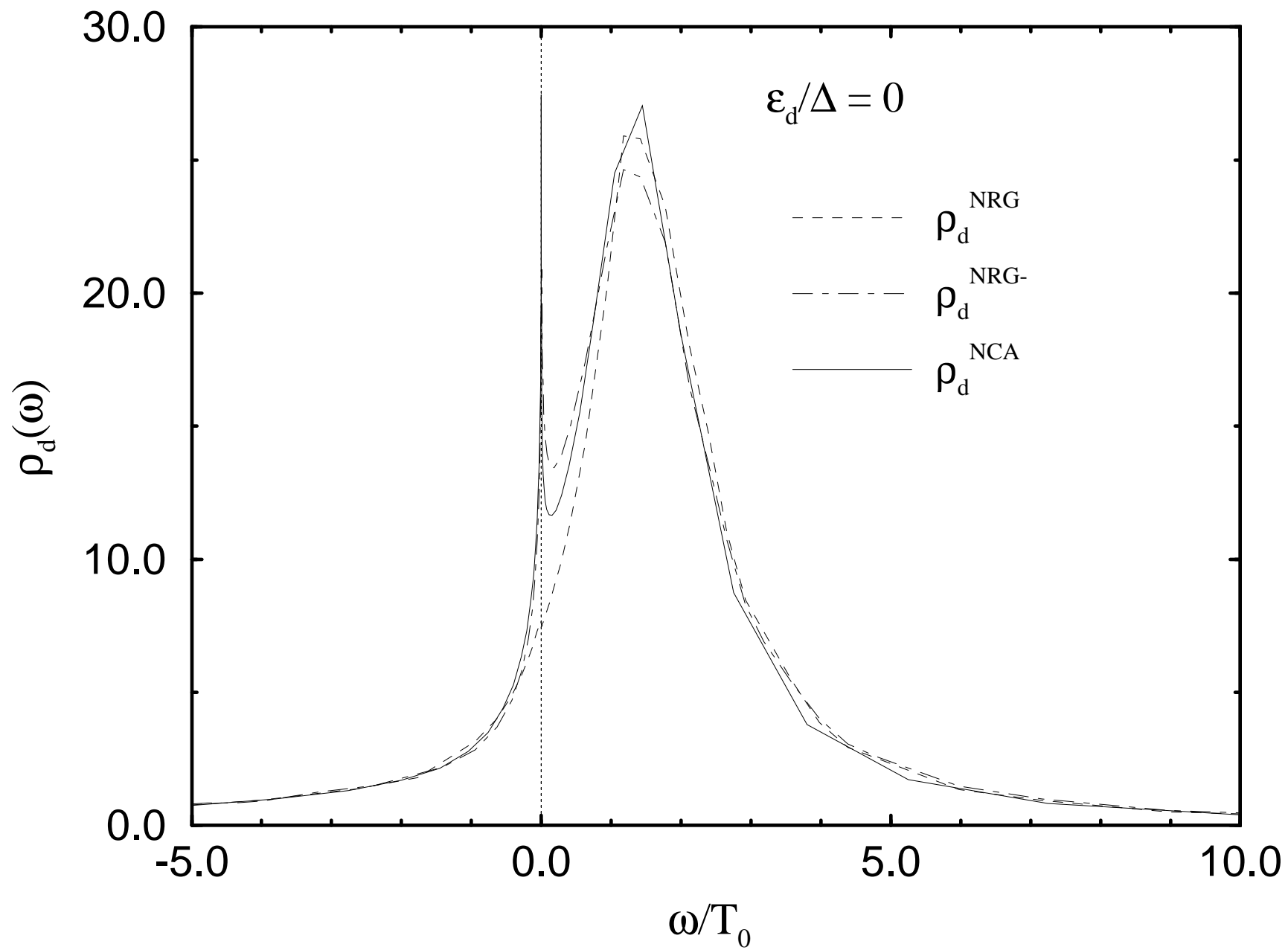




Fig12

